Linköping university
Department of Management and Engineering
Division of Solid Mechanics
Master's thesis, 30 credits | Master programm
Spring 2021 | **LIU-IEI-TEK-A–21/04182-SE**

Study of Diamond Folds in Mass-Impregnated (MI) Cables

Sucheth Krishna Kumar Bysani

Linköping university
Department of Management and Engineering
Division of Solid Mechanics
TQFT30 2021 | Master Thesis Report

Linköping university
Department of Management and Engineering
Division of Solid Mechanics
TQFT30 2021 | Master Thesis Report

Study of Diamond Folds in Mass-Impregnated (MI) Cables

Sucheth Krishna Kumar Bysani

Examiner: Peter Schmidt
Academic supervisor: Lars Johannson
Industrial supervisors: Denny Tjahjanto and Giampaolo Martufi

LINKÖPINGS UNIVERSITET

Linköping university
SE-581 83 Linköping, Sweden
013-28 10 00, www.liu.se

Abstract

High Voltage (HV) cables are designed to transmit electrical power from the source to the place where it is consumed. The global trend towards renewable energy sources e.g. wind farms, hydroelectric and solar panels have led to an increase in the use of HV cables, as these sources are situated in remote locations far from the areas where they are consumed. Therefore. there is a need for developing efficient power transmission cables.

Mass-impregnated (MI) cable is a type of HV cable which contains an electrical insulation layer of oil or mass impregnated cellulose paper. Due to its excellent dielectric properties, MI cables has been established as a solution for high voltage electrical transmission system, which has been used for several decades.

The main area of interest in this thesis is the paper insulation in the MI cable. It is important to ensure that the paper insulation structure is robust enough to avoid any formation of damage and/or defects due to excessive deformations during cable production, handling and installation, which might affect the overall electrical performance of the cable. During handling, the dry lapped cable needs to be bent and unbent several times and there is a risk that the insulation will develop voids due to structural defects, thereby reducing the dielectric capacity of the cable. An example of typical structural defects in MI cables is, so-called, diamond folds, i.e. a collective buckling of several paper strips due to axial compressive load resembling a diamond shaped pattern.

The goal of this thesis work is to contribute to the knowledge of the mechanism of diamond folds in MI cable; the onset of diamond fold and post-buckling responses. The contributions from the cable design or production parameters are also studied. The analyses will be conducted using numerical simulation techniques and will be compared to results from characterization tests already conducted in mechanics lab at NKT Technology consulting.

The results of this thesis has given an insight about the effect of insulation design parameters such as registration, butt-gaps, coefficient of friction and number of layers, on the diamond fold buckling behavior in an MI cable insulation. It is recommended that these parameters have to be carefully controlled so as to avoid formation of diamond fold buckling in the insulation.

Keywords: FEM, MI cable insulation, diamond fold buckling, lapping tension, registration and butt-gap

Acknowledgements

It has been a great learning experience working with the Applied Mechanics department of NKT Technology consulting AB, Västerås. First off, I would like extend my deepest gratitude to my supervisors at NKT, Denny Tjahjanto (Principal scientist of Applied mechanics department) and Giampaolo Martufi (Interim Manager of Applied mechanics department), for giving me this wonderful opportunity of carrying out my master thesis under their guidance. Their constant technical support and feedback has guided me in the right path and has helped me gain a lot of knowledge both personally and professionally. I would like to extend my gratitude to everyone working in NKT Technology consulting AB, Västerås for their active and passive support through the course of my master thesis. I would like to specially thank Thomas Liljenberg, Huang Hui, Yang Zhou, Daniel Morin, Zohreh Keshavarz and Annelie Lonnholm for extending their time and support throughout the course of my thesis.

I extend my sincere gratitude to Lars Johansson, my supervisor at Linköping university, who has mentored me throughout the thesis with his insightful academic and technical suggestions.

I am grateful towards Peter Schmidt, my examiner at Linköping university for his valuable reviews and suggestions towards improving the standard of the thesis.

Ultimately, I would like to express profound gratitude to my parents, sibling, family and friends for providing me with unconditional love and support, encouraging me throughout the process of writing my master thesis.

Nomenclature

Abbreviations and Acronyms

Abbreviation	Meaning
LiU	Linköping University
NKT	Nordiske Kabel og Traadfabriker
DF	Diamond Fold
HVDC	High Voltage Direct Current
MI	Mass Impregnated
HV	High Voltage
XLPE	Cross-linked Polyethylene
MD	Machine Direction
CD	Cross Direction
TD	Through Thickness Direction

Latin Symbols

Symbol	Description	Units
r	Radius of paper cylinder	[m]
r_0	Radius of conductor core	[m]
W	Total width of FE model	[m]
W_P	Width of paper strip	[m]
t	Thickness	[m]
P	Pressure	[Pa]
E	Young's modulus	[Pa]
G	Shear modulus	[Pa]
σ_y	Yield strength	[Pa]
σ_u	Critical stress	[Pa]
F_{crit}	Critical force	[N]
u	Displacement field	
ϑ	Rotational field	

Greek Symbols

Symbol	Description	Units
μ	Micro (1e-6)	[0]
ν	Poisson's ratio	

Contents

List of Figures

List of Tables

1 Introduction

1.1 About NKT

Nordiske Kabel og Traadfabriker, NKT, is a pioneer in power cable technology with a vision of connecting societies to a greener world by enabling sustainable energy transmission. The company was founded by H.P. Prior in 1891, a ship owner who saw a potential market for making high quality wire for power distribution and for the new-fangled telephone. H.P. Prior was a visionary and an industrialist of the 19th century who paved a way of life towards a degree of comfort and convenience of the modern world running on electrical power.

NKT has a footprint in more than 14 countries and has manufacturing facilities in Germany, Sweden, Poland, the Czech Republic, Norway and Denmark. NKT is continuously developing innovative and sustainable methods of power transmission to drive the world in the digital age of the fourth industrial revolution and the global transition to renewable energy.

NKT has many accolades to its name. It launched the first HVDC MI submarine cable connecting Gotland with the Swedish mainland in 1954 and recently it developed the largest submarine cable in the world with a diameter of around 270 mm. With its vision of connecting a greener world, NKT has taken all possible and necessary actions to reduce its impact on the climate and to strengthen its social impact. Innovations in cable technology manufacturing, by utilizing renewable sources of energy for production and recycling cable scrap are some of the major steps taken by the company to reduce its carbon footprint [1].

1.2 Background

1.2.1 High voltage cables

A high voltage (HV) cable is designed to transmit electric power at high voltage from a source to a place where it is consumed. High voltage cables consist of several components such as a conductor, insulating system and protective jackets. HV cables are used either as underground or submarine cables. Impregnated paper along with cross-linked polyethylene (XLPE) insulating systems are currently the most common type of insulations in use, with impregnated paper being the most popular option for direct current (DC) transmission. It is predicted that with further advancements in the XLPE systems it is estimated to make up about 50 to 70 per cent of new cable installations in the HV range [2], [3].

1.2.2 Mass-impregnated (MI) cables

The use of oil impregnated or mass impregnated paper insulation dates back to 1885 with the first such cable being used in 1872 [2]. Oil or mass impregnated paper is the most widely used insulation system in HV cables and involves lapping of paper strips around the conductor core and impregnating it with a certain type of mineral oil, so as to build up an effective insulating system. Oil impregnation adds further complexity to the problem and its effect will be neglected in the analysis. Hence, a dry lapped paper insulation is considered for this thesis.

MI cable consists of several parts which are necessary for efficient transmission of power through the cable. Cross section of an MI cable is as shown in Figure (1):

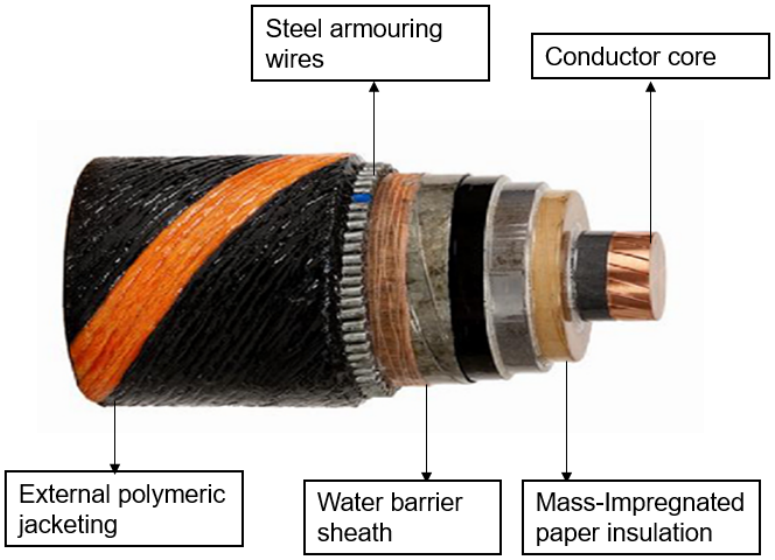

Figure 1: Schematic representation of the conductor, paper insulation and protective layers in an MI cable

The main parts of an MI cable are [4]:

1. Conductor: The conductor core is made up of solid or helically-wound strands of copper or aluminium. The purpose of the conductor is to transmit electrical power.

2. Insulation layers: MI cable insulation consists of helically-wound dry-lapped paper strips impregnated with mineral oil. Insulation layers reduces the electrical transmission losses as it is dielectric in nature.

3. Protection or armouring layers: For the purpose of protecting the cable from harsh external conditions, the MI cable consists of components such as cable armouring layer, water barrier sheath, tensile armour wires and external polymeric jacket.

From a mechanical point of view the insulation system is of greatest interest. This is because the insulation layers must be mechanically robust in order to ensure that it can deliver its electrical performance; mechanical damage and instabilities, e.g. buckling and creasing, could potentially degrade the overall electrical properties of the insulation layer.

1.3 Problem description

Most MI cables are used in submarine and underground applications and hence lengthy cables have to be transported to these places as efficiently as possible. It would be ideal if the diameter of the capstan or the reel on which the cable is wound is large enough to make sure that the deformation of the insulation produced by bending could be maintained well below the elastic limits of paper [9]. When the cable is bent beyond its critical radius i.e. bending radius above which the cable will undergo damage, the compressed part of the cable undergoes different types of damage which can result in the total loss of the cable.

Damage to the insulation in an MI cable can also occur during its manufacturing, handling and installation. Hence the design parameters of the cable have to be selected such that the cable is mechanically robust enough to not undergo any form of damage of the paper insulation.
Some of the common forms of damage seen in an MI cable insulation are [5]:

1. Butt-space creases: These occur in the compressed part of the insulation where the end thrust on the paper are large enough to overcome the frictional forces between the paper layers and result in a collapse as shown in Figure (2a).

2. Collapse creases: These occur in the compressed zone when the paper tapes not only collapse in the butt-gaps but also outside it. They are characterized by complete collapse of a considerable thickness of the insulation and appear in the form of buckling with sharp edges. Figure (2b) shows an MI cable with collapse crease type of deformation.

3. Diamond folds: A diamond fold is one particular type of thin-walled cylinder buckling, where the buckling mode resembles diamond shapes in chequerboard pattern, as shown in Figure (2c).

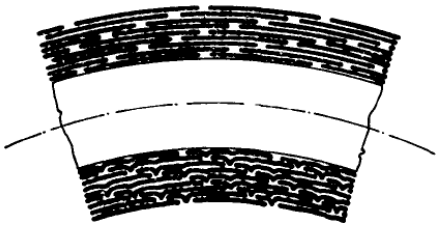

(a) Butt-space creases

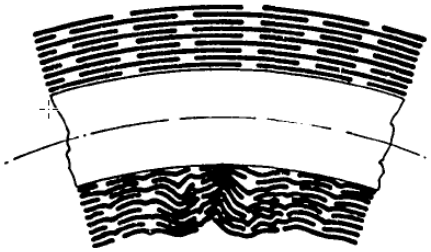

(b) Collapse creases

(c) Diamond fold buckling

Figure 2: Common forms of buckling damage occurring in an MI cable insulation

Any sort of crease or wrinkle deformations in the paper insulation leads to in-homogeneity in contact or interfacial pressure between the paper strips, resulting in gaps or separation between paper layers. Separation between the layers leads to formation of cavities or oil pockets between the layers. The combination of cavities and variation in electric fields can result in loss of efficiency of power transmission through the cable. Hence any forms of damage on the insulation has to be avoided so as to maintain the functioning of the cable [5].

This thesis will mainly focus on one type of damage in the MI cable called diamond folds buckling and aims on building knowledge on the detailed mechanism of diamond folds in MI cable insulation.

1.4 MI cable insulation

MI cable insulation consists of helically-wound dry-lapped paper strips impregnated with mineral oil. Figure (3) schematically illustrates the configuration of stack of paper strips in an MI cable insulation. Let r_0 be the radius of the conductor. The overall thickness of the insulation layer is defined as $r - r_0$, where r is the outer radius of the insulation layer. The thickness of the individual paper strip is denoted by t and the width of the paper strip is W_P. The paper strips are stacked in a specific configuration, called *registration*; it describes the ratio of the overlapping area between adjacent paper strips, i.e. $W_{P1} : W_{P2}$.

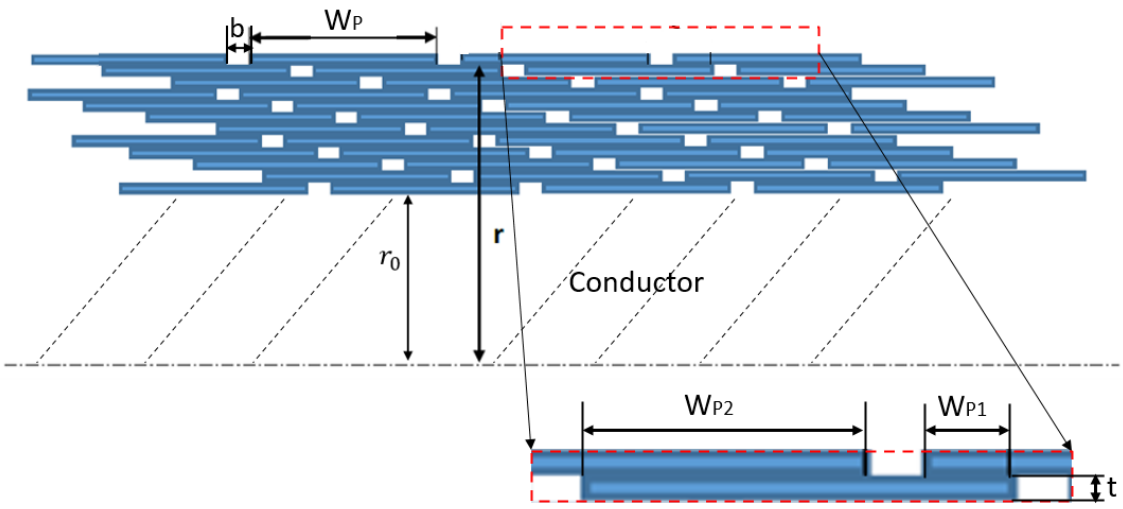

Figure 3: Configuration of stacked paper strips in an MI cable insulation

Several factors might have an affect on the buckling behaviour in the cable, some of which are:

1. Lapping tension: The paper is wound with a certain amount of tension, which generates interfacial pressure between paper layers.

2. Paper strip dimension: The dimensions (width (W_P) and thickness (t)) of a paper strip are also parameters which might affect the diamond fold buckling behaviour of the insulation. The effect of thickness of a paper strip is investigated in the sections to follow.

3. Butt-gap: Butt-gap is a small gap between two successive paper strips. Butt-gaps are necessary for the bending of the cable, without which the cable will become very stiff and lead to logistical issues. Variation of size and positioning of the butt-gaps might also affect the DF buckling behaviour in the paper insulation. In order to reduce the number of

variables on which the buckling behavior depends, the size of the butt-gap is kept constant at 2 mm throughout the thesis.

4. Registration: The paper strips are stacked in a specific configuration, called *registration*; it describes the ratio of the overlapping area between adjacent paper strips, i.e. $W_{P1} : W_{P2}$. Figure (4) shows an example of a 30-70% registration pattern applied on paper strips. Consider three paper strips A, B and C of certain width W_P. Paper strips A and B are separated by a small gap of 2 mm called butt-gap. If 30-70% registration scheme is applied to the paper strips, excluding 2 mm dimension of the butt-gap, 30% of the width (W_P-b) of paper strip C overlaps strip A, while the remaining 70% of the paper strip overlaps strip B.

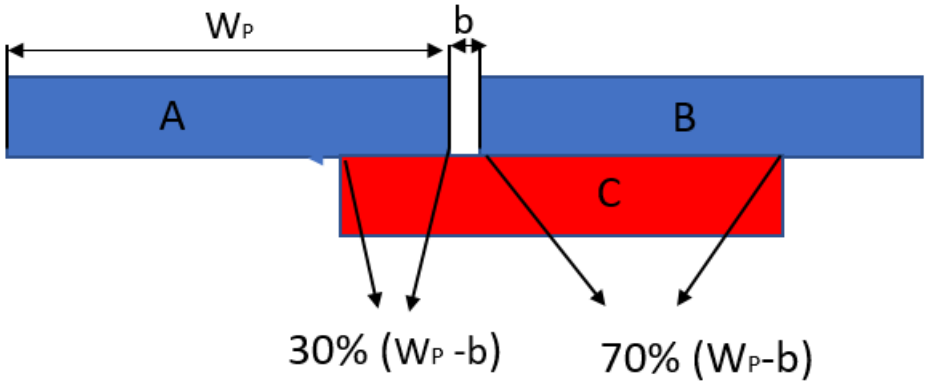

Figure 4: Example of 30-70 registration scheme

1.5 Objectives

The main objective of the thesis is to develop detailed knowledge on diamond folds phenomenon in an MI cable insulation. Particular interest is given on determining the onset of diamond fold buckling as well as the corresponding post-buckling behaviour by means of modelling and numerical techniques. The effects of the above mentioned parameter (registration, paper strip dimensions, butt-gap and lapping tension) onto the overall diamond fold buckling characteristics are studied in detail.

2 Methodology

In this study, in order to avoid instability of the solution during numerical simulations, initially a buckling modal analysis (eigenvalue analysis) is performed on a perfect geometry of the paper insulation. A number of different buckling phenomena for e.g. corrugations and diamond folds are observed in the modal analysis. An eigenmode corresponding to the required diamond fold configuration is seeded on to the FE model and a FE analysis is carried out.

When the applied compressive force reaches a critical value i.e. the force at which buckling takes place, the specimen which is under elastic compression buckles [5], [6]. This transition from an elastic loading to buckling can be seen in the stress strain plot for the specimen. The maximum stress at which the transition from elastic region to buckling region takes place indicates critical stress of buckling [5].

A parametric study is carried out on the design parameters (registration, paper strip dimensions etc) for single and multi-layers of paper insulation. The critical stress of buckling for each of the parameter is compared to understand its effect on the DF buckling behaviour in the paper insulation.

A parametric study on lapping tension and friction coefficient between layers, is carried out on a FE model with four layers of paper insulation. By comparing the critical stress from several analyses, conclusions can be drawn on the effect, lapping tension and friction coefficient have on the critical stress of diamond fold buckling.

The effect of registration and butt-gaps are investigated on a FE model resembling an actual MI cable insulation. Keeping coefficient of friction and number of layers constant, interfacial pressure is varied and its effect on the behaviour of the model is studied

The results obtained from the parametric studies are compared with experimental test results obtained from compression tests carried out in mechanics labs at NKT Technology Consulting.

3 Theoretical framework

3.1 Buckling in thin-walled cylinders under axial load

As described in the introduction, the paper strips are wound with a certain tension, hence exerting pressure on the underlying paper strips. The applied radial pressure presses one layer against another, leading to frictional forces between the layers when the cable is bent. During bending of the cable, the top half of it is in tension while the bottom half is in compression. In tension, the forces in the slipping direction tend to pull the paper strips away from each other, in contrast to the compressive forces which tends to push the strips towards each other [5]. In order to simplify, and since the phenomenon investigated here occurs only in the compressed part of the cable, the problem of bending is idealized by considering it as axial compression of a thin walled cylinder [5].

The first attempt towards developing a theoretical model to predict the critical stress was by R. Lorenz in 1908, who developed the classical buckling theory for the axisymmetric deformation of a thin walled cylindrical shell with simply supported edges, subjected to uniform axial compression [7]. In 1910, S.P. Timoshenko derived the classical buckling formula using the energy method and by solving the eigenvalue problem defined by a fourth order equilibrium equation and boundary conditions [7].

The classical theory by S.P. Timoshenko was based on the assumptions of perfect initial shape and infinitesimal deflections on the surface of the cylinder. S.P. Timoshenko derived the formula on the assumption that, when a thin cylindrical shell is uniformly compressed in the axial direction, symmetrical buckling with reference to the axis of the cylinder will occur at a certain value of the compressive load [8]. S.P. Timoshenko uses the strain energy method to obtain the value of the critical load and assumed that in the unbuckled state, the total strain energy in the cylinder is the energy due to the axial compression [8]. When the compressive load reaches the critical value, the strain energy of the shell increases and must be equal to the work done by the compressive load [8]. The formula for critical stress according to the classical theory is as follows:

$$\sigma_u = \frac{1}{\sqrt{3(1-\nu^2)}} \frac{Et}{r} \tag{1}$$

The critical stress according to Eqn. (1), is a function of the Young's modulus (E), thickness (t), radius of the cylinder (r) and Poisson's ratio (ν).

Donnell compared the results of experiments on axial loading cylindrical shells with the results from the classical theory and observed that the ratio of the experimental buckling stress to the theoretical stress was approximately found to be one half to two thirds [9], [10]. There was also a great discrepancy between the final and predicted shapes of buckling in the cylindrical shells [10]. The main reason for the discrepancy in the theoretical and experimental results was because the classical theory was developed assuming that the initial shape of the specimen was perfect and it had infinitesimal deflections [7], [9], [10]. The classical theory did not take into account the small imperfections present on the cylinder and due to this the predicted critical stress served as an upper limit for buckling.

Based on the experimental results, Donnell formulated an empirical model to determine the critical stress of buckling. In contrast to the classical buckling theory, the empirical model considered the effect of initial deflection on the cylindrical model. When an axial compressive load is applied to the cylinder, these initial deviations on the cylinder are increased and the stresses due to the imperfections increases rapidly. The cylinder reaches the yield point of paper at certain points (locally) much lower than the value predicted by the classical buckling theory.

Further increasing load after this point, it is evident that the resistance of the cylinder will rapidly fall and the whole structure will buckle [9]. The model was based on the assumption that the critical stress was a function of the yield point (σ_y), modulus of elasticity (E) and the thickness-radius ($\frac{t}{r}$) ratio. The empirical formula formulated by Donnell to determine the critical stress of buckling is as follows:

$$\sigma_u = E\frac{0.6\frac{t}{r} - 10^{-7}\frac{r}{t}}{1 + 0.004\frac{E}{\sigma_y}} \tag{2}$$

Both the classical and Donnell models were developed for an isotropic material. A theoretical model to obtain the critical stress of buckling in paper cylinders was developed by Paolo Gazzana Priaroggia et.al in 1961 [5]. The theory was based on the assumption that when a cable is bent, the maximum axial deformation due to it is larger than the elastic limit of paper but is within the limit corresponding to the disappearance of butt-spaces in the compressed zone of an insulation system. Critical stress was obtained using the formula :

$$\sigma_u = \frac{1}{\sqrt{3}}\frac{t}{r}\sqrt[4]{G^2 E_\Theta E_Z} \tag{3}$$

Critical stress from Eqn (3) is a function of thickness (t), radius (r), shear modulus (G) and Young's modulus (E) in the Θ and the Z directions. The presence of G, E_Θ and E_Z terms in Eqn (3) represent the anisotropic material properties of paper. This theoretical model (Eqn 3) will be referred to as Pirelli model throughout the thesis.

According to the equations (1), (2) and (3), critical stress of buckling is a function of Young's modulus (E) of the material, radius of the thin cylinder (r) and thickness of the thin cylinder (t). It is mathematically challenging to obtain the analytical expressions for the critical stress for the actual MI cable insulation situation that account for the interactions between adjacent paper strips. Hence, numerical models will be employed to investigate the effects of radial interfacial pressure, registration, friction coefficient between layers onto the overall diamond fold buckling response in an MI cable insulation.

4 Finite element modelling

4.1 Numerical simulation procedure

Buckling is a non-linear problem. Solving buckling numerically can be challenging due to instability of the solution. Hence, initial imperfections are introduced in order to circumvent these issues [11], [15]. A step by step description about the method used for numerically capturing diamond fold buckling behaviour in a thin cylindrical shell is as follows:

1. In the first step, a mode-shape analysis is carried out on the ideal geometry to establish buckling modes. Initial geometrical imperfections will be selected from the sets of mode-shape analysis solutions, such that it corresponds to the experimentally observed diamond fold pattern.

2. Static boundary value problems are solved for buckling of thin-walled cylinders under axial compression load, where geometrical imperfections have been applied as the initial conditions. The magnitude or size of the initial imperfections is determined such that it is sufficiently large enough to obtain a smooth buckling response, but small enough to ensure the accuracy of the solution.

3. The force displacement curve is converted into stress strain response. Onset of instability in the stress strain response indicates, critical stress of diamond fold buckling.

4.2 Geometrical aspects

In the scope of the thesis, it is assumed that diamond fold buckling under uni-axial compression is symmetric about its axis. Therefore, only a quarter of a cylinder is modelled in the present work, in conjunction with the applications of symmetric boundary conditions. This in turn minimises the computational resources allocated for each analysis of the model.

Two kinds of geometries will be investigated in the course of this thesis. The geometries are as follows:

1. Continuous cylinder as seen in Figure (5a).

2. Stack of paper strips with butt-gaps as seen in Figure (5b).

The second model is aimed at mimicking the geometry of an actual MI cable insulation, while the first model is a simplification of the later. Total width (W) of both the models was fixed to 58 mm.

As mentioned in earlier sections, paper insulation is modelled as a shell and the thickness of the shell or cylinder is set to 0.1 mm, corresponding to the actual thickness of the paper strips.

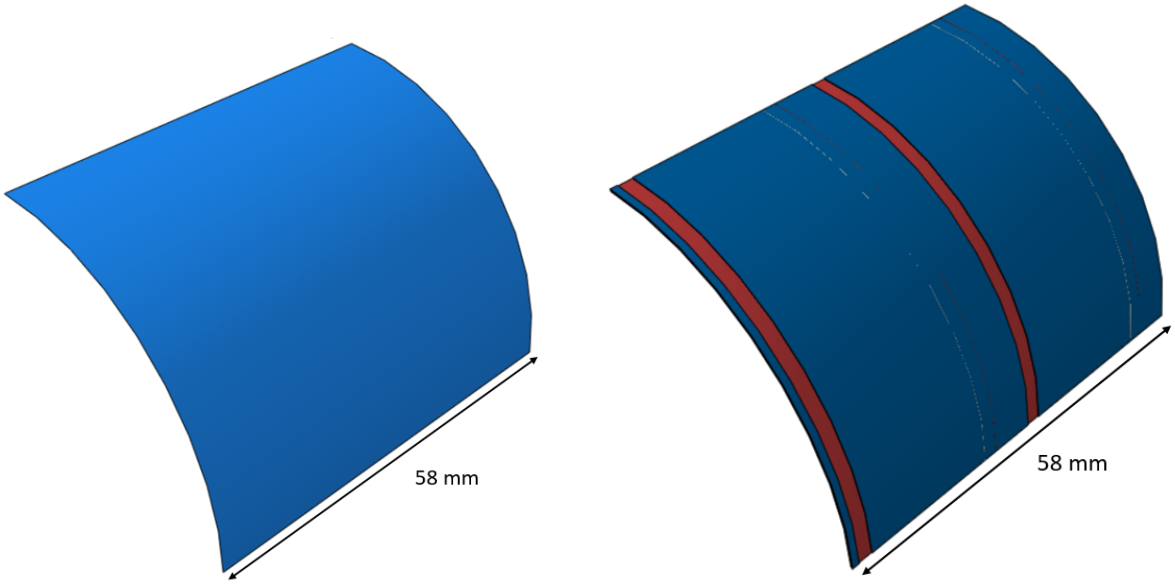

(a) Continuous thin-walled cylinder geometry

(b) Over-lapping paper strips stacked in a certain registration. The model consists of four layers of paper insulation

Figure 5: Geometrical models for both the cases. Total width (W) of the FE model is 58 mm

4.3 Material properties of paper

Paper exhibits a strong anisotropic behaviour, due to its micro structure topology, i.e. porous network of cellulose fibres. Anisotropy or directionality refers to a phenomenon where the material properties such as the elastic constants, of a material differ along different directions [12]. The three principal directions in paper are the machine direction (MD), cross direction (CD) and the through thickness direction (TD) [12]. Machine direction is the direction in which the fibres of paper are oriented. Paper exhibits superior elastic strength in the MD when compared to the CD. In an actual MI cable insulation, paper strips are wound in the machine direction while the compressive load leading to buckling is applied through the cross direction. Figure (6a) shows a schematic representation of the anisotropic directions of paper.

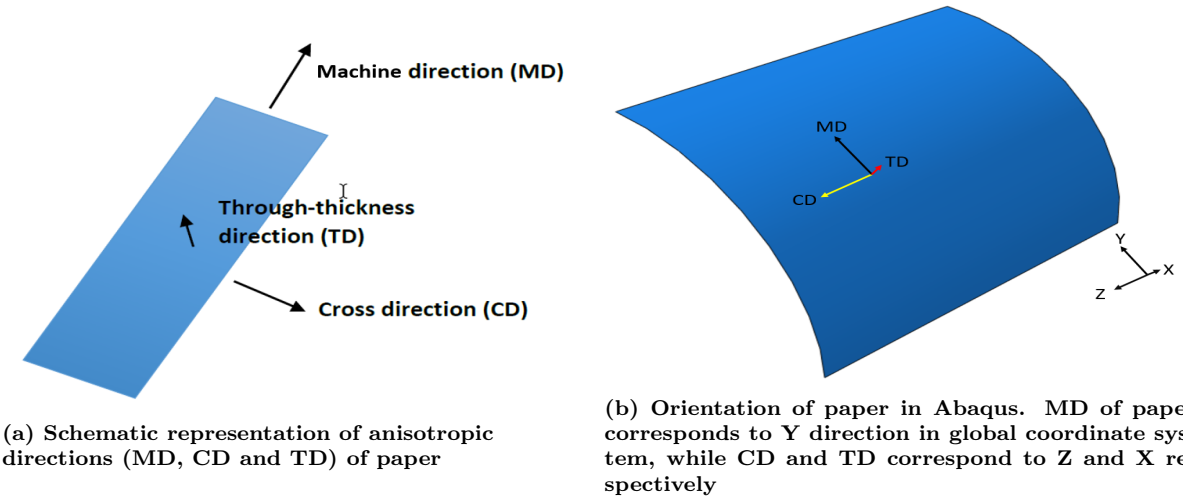

(a) Schematic representation of anisotropic directions (MD, CD and TD) of paper

(b) Orientation of paper in Abaqus. MD of paper corresponds to Y direction in global coordinate system, while CD and TD correspond to Z and X respectively

Figure 6: Depiction of anisotropic directions of paper

Figure (6b) shows how the material is oriented to the FE model in Abaqus. Using the orientation command, the anisotropy of the material is applied to the model.

The values for the elastic constants are obtained from various tensile tests performed within NKT. The elastic constants for paper are:

Material Parameters	Paper Directions		
Young's Modulus	E_{MD}	E_{CD}	E_{TD}
	10 GPa	4.5 GPa	100 MPa
Poisson's ratio	$\nu_{MD–CD}$	$\nu_{MD–TD}$	$\nu_{CD–TD}$
	0.2	0	0
Shear modulus	$G_{MD–CD}$	$G_{MD–TD}$	$G_{CD–TD}$
	3 GPa	100 MPa	100 MPa

Table 1: Elastic constants of paper

4.4 Boundary conditions

Since only a quarter part of the cylinder is modelled, symmetrical boundary conditions will be applied to the model, to obtain a realistic response. Figure (7) shows the FE model with four sides A, B, C and D.

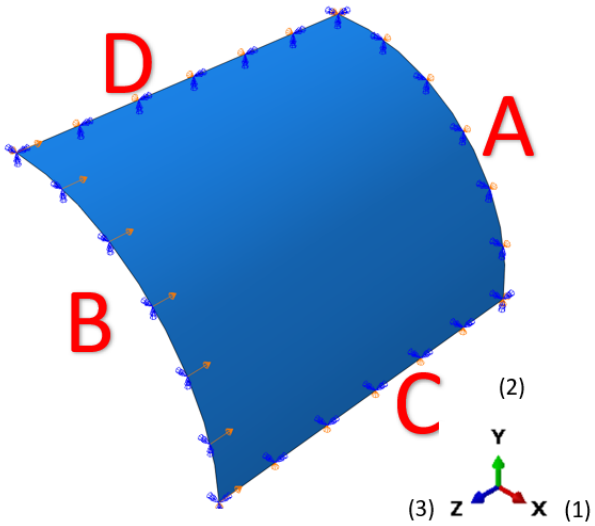

Figure 7: Boundary conditions applied to the FE model. A, B, C and D represent the sides of the quarter cylinder model

The FE model consists of four sides A, B, C and D and the boundary conditions applied on each of these sides is as shown in table:

Side	Boundary Condition
A	$u_Z = \vartheta_X = \vartheta_Y = 0$
B	$\vartheta_X = \vartheta_Y = 0, u_Z = -0.1\text{mm}$
C	$u_Y = \vartheta_X = \vartheta_Z = 0$
D	$u_X = \vartheta_Y = \vartheta_Z = 0$

Table 2: Boundary conditions applied to the FE model

In the table, u indicates displacement while ϑ indicates rotation DOF. The Z displacement along with the X and Y rotations are constrained on side A, while side B also has its X and Y rotations constrained but is applied with a displacement of 0.1 mm in the negative Z direction. On C, Y symmetrical boundary conditions are applied i.e. Y displacement along with X and Z rotations are constrained; whereas the constraints applied on side D resemble X symmetry, with the X displacement, Y and Z rotations constrained.

4.5 Mesh sensitivity analysis

In general, mesh sensitivity analysis is carried out to make sure that the results that are obtained are due to the boundary conditions and physics used, not the mesh resolution [13]. Hence, in order to understand the sensitivity of the mesh configurations on the result, a mesh sensitivity analysis will be carried out to check the dependency of the result on the mesh configuration and a good mesh configuration will be chosen.

Shell elements were used for analysis of buckling behaviour in this study. An element is considered thin if its thickness is less than $1/10^{\text{th}}$ of its radius [13]. Since the considered paper thickness is 0.1 mm, it satisfies the condition for considering it as a thin shell application. Therefore, a thin shell approximation is used for this analysis [13]. Five integration points with Simpson rule of integration are defined through the thickness of the shell.

The shell element class is further subdivided into two main groups- linear and quadratic elements. For the mesh sensitivity analysis linear and quadratic quadrilateral element along with linear triangular elements will be studied.

Important characteristics of the three element types considered are:

- Linear quadrilateral element: Linear quadrilateral shell element contains 4 nodes of integration and uses linear interpolation or shape functions for the displacement field. Full integration scheme is considered in order to minimize the effects of the hour-glass stiffness onto the overall stiffness matrix of the system [14]. Linear quadrilateral element in Abaqus is called as S4. A schematic representation of the element is as shown in Figure (8a).

- Quadratic quadrilateral element: Employs 8 nodes of integration with 5 degrees of freedom (3 translational and 2 rotations) per node . The element is based on quadratic interpolation or shape functions for the displacement field. In the quadratic elements, reduced integration scheme is used for efficiency [14]. Quadratic quadrilateral element in Abaqus is called as S8R5. A schematic representation of the element is as shown in Figure (8b).

- Linear triangular element: Element type contains 3 nodes of integration, with linear interpolation or shape functions. Similar to the linear quadrilateral element, it uses full integration instead of reduced integration. The linear triangular element is called as S3 in Abaqus. A schematic representation of the element is as shown in Figure (8c).

Four element sizes i.e. 0.5×0.5, 0.75×0.75, 1×1 and 1.5×1.5 mm are considered for each of the element types. Critical stress at buckling is used as comparative parameter to compare the effectiveness of each of the mesh configurations.

It is very important that for every analysis the same diamond fold configuration is chosen, because as the configuration changes the critical stress also changes. This point is investigated in the sections to follow. Assuming that the effect of the DF configuration is known, for the mesh sensitivity analysis a DF configuration is chosen. An eigen mode consisting of 1.5 DF cells along the paper width and 10 DF cells along the circumferential direction is chosen for the analysis and is as shown in Figure (9). Valley (blue region) or peak (red region) in Figure (9) corresponds to 0.5 cell of diamond fold, so 1 diamond fold cell will consist of a peak as well as a valley. This eigenmode is chosen because the DF configuration in this mode corresponds to the DF configuration obtained from the experiments.

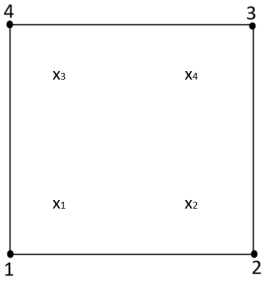

(a) Linear quadrilateral element (S4). Consists of 4 nodes of integration.

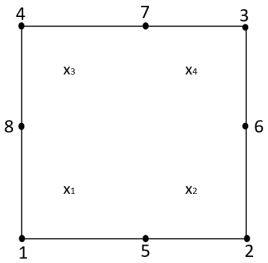

(b) Quadratic quadrilateral element (S8R5). Consists of 8 nodes of integration.

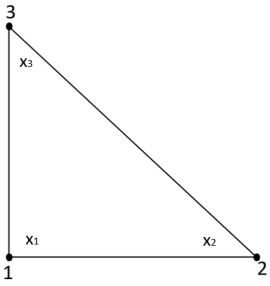

(c) Linear triangular element (S3). Consists of 3 nodes of integration

Figure 8: Schematic representation of the types of elements used in the mesh sensitivity analysis. Black dots on the element represent the nodes of the element. Symbol x represents the points of integration

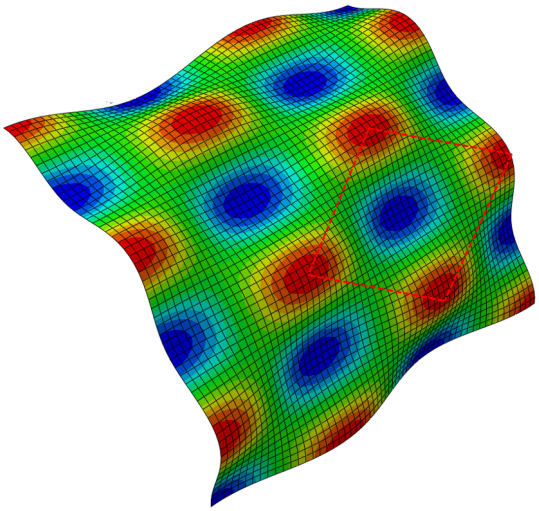

Figure 9: Eigenmode shapes resembling a typical diamond fold buckling pattern that are considered as the reference imperfection geometry in the present analysis.

Figure (10) shows a plot of the stress-strain response for all the mesh configurations. Mesh convergence is studied by plotting the element size along the X-axis and corresponding critical stress on the Y-axis and resulting plot is as seen in Figure (11). Theoretical critical stress from Eqn (3) is 2.9 MPa. Except for a coarse resolution with 1.5×1.5 mm element size, the relative variation of result for subsequent mesh resolutions is between 0-5% and since the variation is within acceptable tolerance, it can be concluded that all the three element types exhibit mesh convergence.

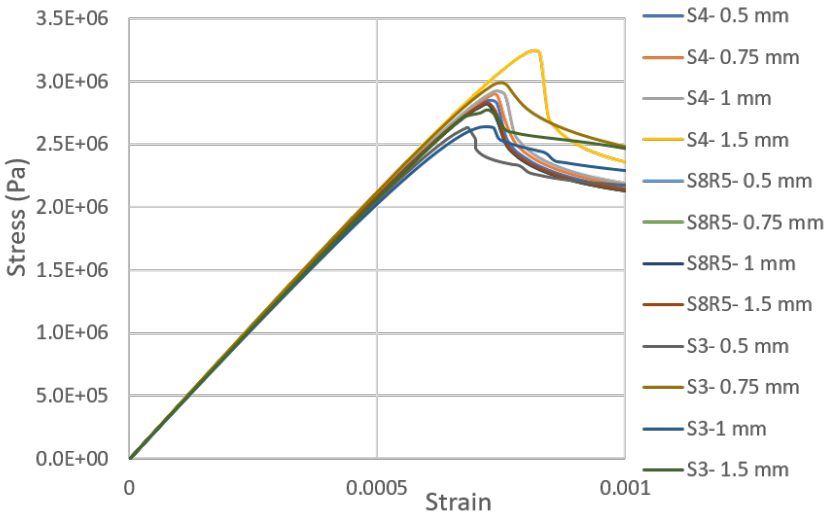

Figure 10: Stress strain response of all the mesh configurations. Due to space constraints in the legend, linear quadrilateral element is represented as S4, quadratic quadrilateral element as S8R5 and linear triangular element as S3. The element dimensions are also represented by a single dimension

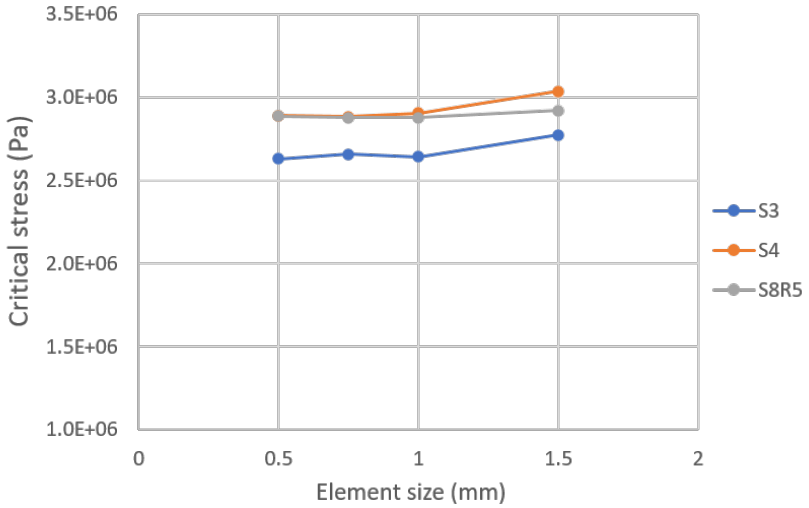

Figure 11: Plot of critical stress against element size for all the three element types indicating mesh convergence

Next, a single mesh configuration has to be selected which gives accurate results and also minimizes the computational resources used for each analysis. From Figure (11) it is seen that the linear and quadratic quadrilateral elements converge onto a critical stress of around 2.85 MPa and the linear triangular element onto a critical stress of around 2.7 MPa. Even though the linear triangle element shows mesh convergence, it under estimates the critical stress for the thin cylinder under axial compression.

Quadratic quadrilateral element is computationally more expensive than linear quadrilateral element; hence linear quadrilateral element is chosen over the quadratic element. The linear quadrilateral element shows mesh convergence from a mesh resolution of element size 1×1 mm, hence this mesh configuration will be used for all the further analysis.

5 Diamond fold buckling of a single-layer cylinder

5.1 The effects of diamond fold cell size

NKT has developed a testing method to axially compress dry lap insulation to observe and measure diamond fold initiation. In the axial direction, 1.5 diamond fold cells were observed along the paper width (W), whereas about 10-14 diamond fold cells were observed along the outer circumference. This configuration will be considered as the reference for FE simulations.

To understand the effect of diamond fold cell size on the critical stress of the model, six different diamond folds configurations with varying number of diamond folds along the paper width and circumference are considered and the DF configurations are as shown in Figure (12):

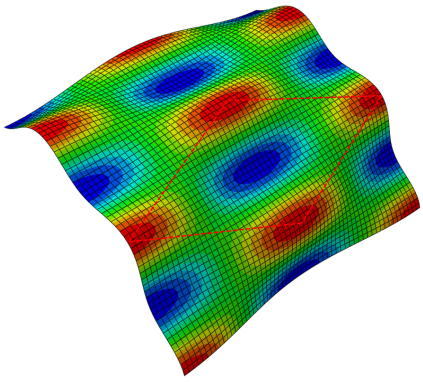

(a) 1 cell along the paper width (W); 2.5 cells in circumferential direction

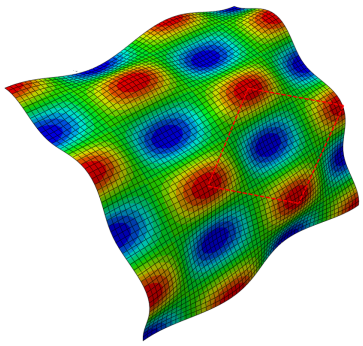

(b) 1.5 cells along the paper width (W); 2.5 cells in circumferential direction

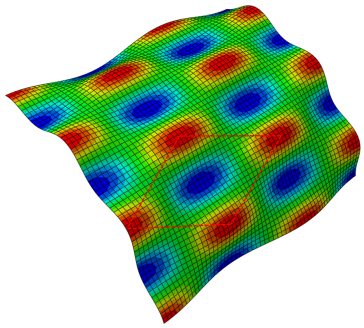

(c) 1.5 cells along the paper width (W); 3 cells in circumferential direction

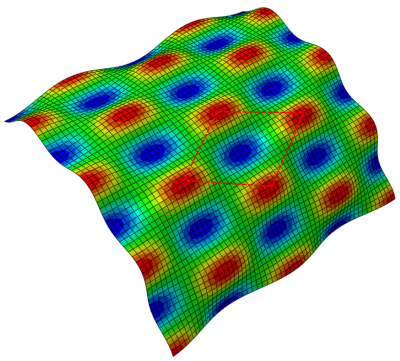

(d) 2 cells along the paper width (W); 3.5 cells in circumferential direction

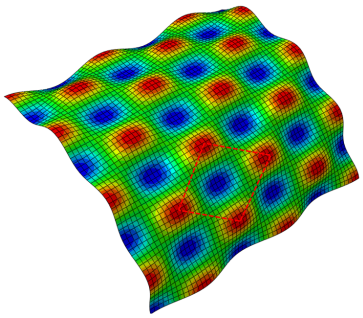

(e) 2.5 cells along the paper width (W); 3.5 cells in circumferential direction

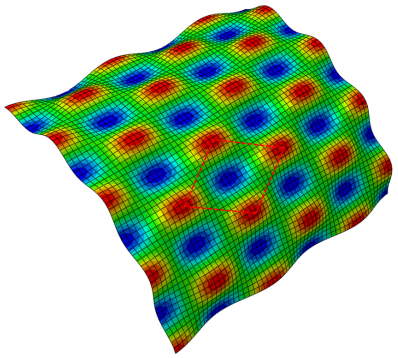

(f) 2.5 cells along the paper width (W); 4 cells in circumferential direction

Figure 12: Six diamond fold configurations with varying cell size and numbers along the paper width (W) and circumferential direction (of a quarter circumference model)

FE analysis are carried out for all these configurations and the resulting stress-strain curves are plotted in Figure (13a). Critical stresses are extracted for each of the diamond fold cell size and the variation of critical stress with diamond fold cell size is as shown in Figure (13b). The comparison from Figure (13b) shows that the critical stress of the model is dependent on the diamond fold cell size. A mode having smaller diamond fold size will exhibit greater resistance to buckling when compared to a mode having larger diamond fold cell size. It therefore becomes important that for future analyses the DF configuration chosen should relate to the configuration obtained from the experiments.

The eigenmode with 1.5 diamond fold cells along the paper width (W) and 10 diamond fold cells in circumferential direction closely matches with the experimental configuration. This configuration will be carried forward for all the further analyses. The chosen diamond fold configuration with 1.5 diamond fold cells along the paper width (W) and 10 diamond fold cells along the circumference is as shown in Figure (12b).

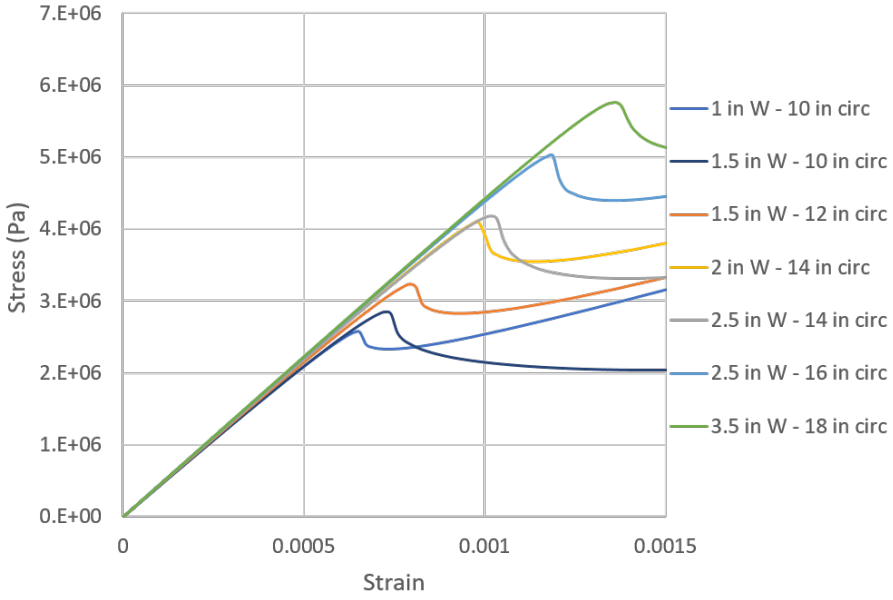

(a) Plot of stress strain response for each of the diamond fold configuration

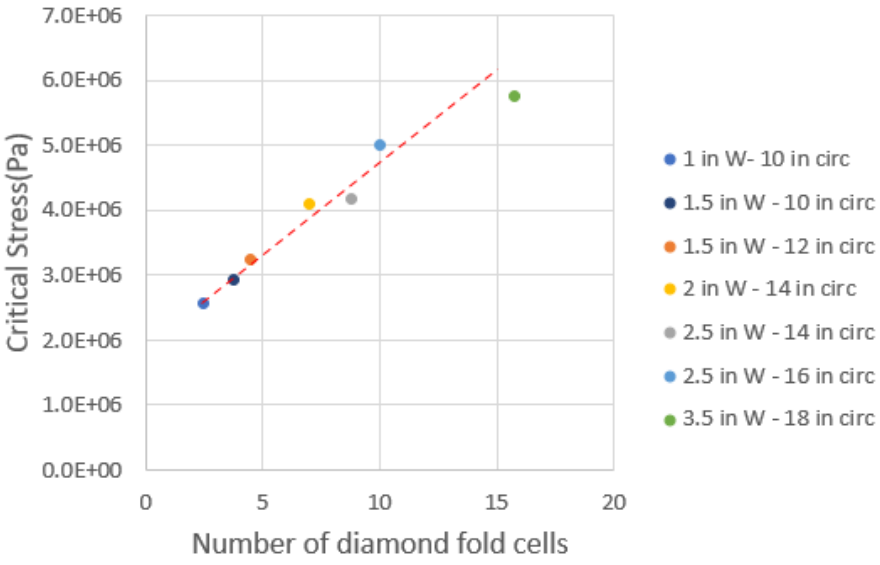

(b) Plot of number of diamond fold or cell size with its corresponding critical stress

Figure 13: Results for the effect of diamond fold cell size. Legend indicates the number of DF cells along the paper width (W) - number of DF cells in the circumferential direction.

5.2 The effects of cylinder size (cylinder radius)

In this section, a parametric study on the effect of cylinder radius on the critical stress of the model is studied. The analysis is carried out for material properties of steel and paper and the results are compared with the critical stress from equations (1), (2) and (3). This analysis will give an insight about the the pros and cons of each of the theoretical and empirical models as outlined in the theory section.

For the case of steel, Young's modulus is assumed to be 200 GPa, while its yield strength is 200 MPa and 80 GPa is its shear modulus. A parametric study on the radius of cylinder is carried out for 25, 35, 45 and 55 mm with steel material properties and the resulting critical stress is compared with the results from the equations (1), (2) and (3).

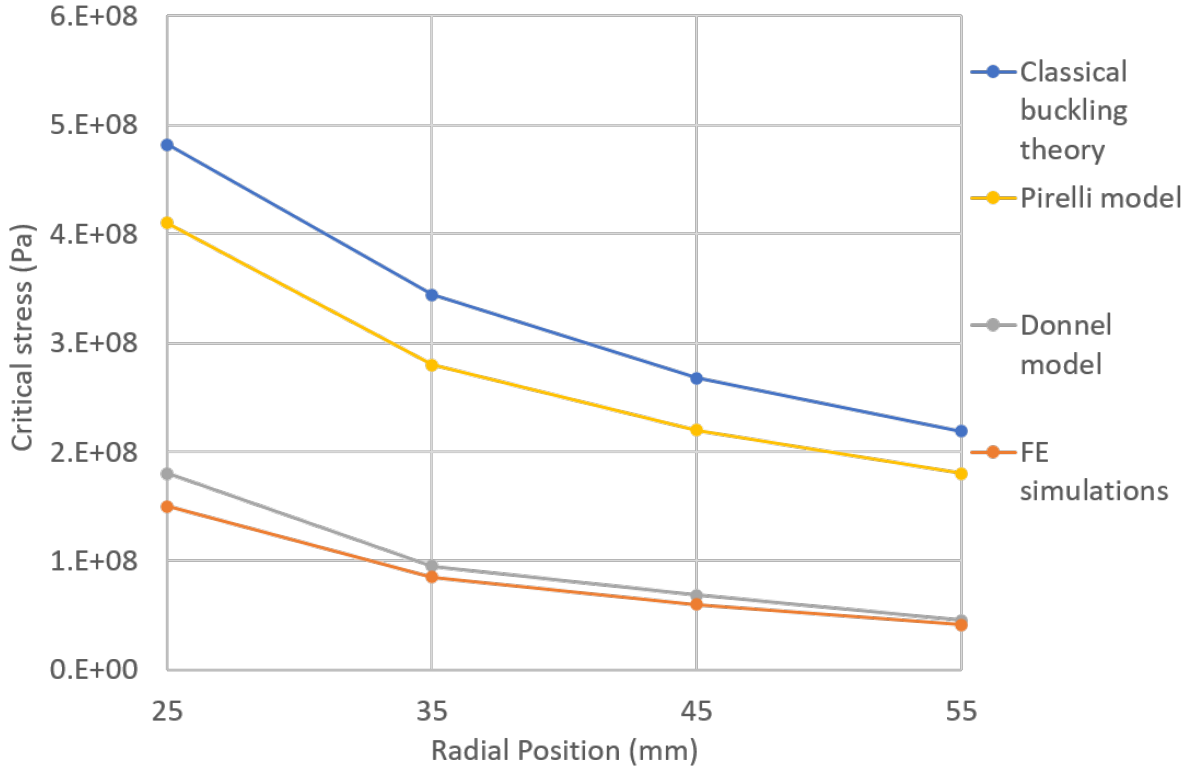

Figure 14: Variation of critical stress with cylinder radius for steel material properties. Comparison of results from equations (1), (2), (3) and FE simulations

Figure (14) shows a comparison of the critical stress obtained from FE simulations with the results obtained from equations (1), (2) and (3). The trends from Figure (14) indicate that the critical stress of the model decreases with increase in the radius of the cylinder. The FE results are nowhere near the critical stress predicted by the classical buckling theory and the Pirelli model. FE results are in good agreement with the Donnell model. As stated earlier, the critical stress by classical buckling theory is like an upper limit for buckling while the Pirelli model might not be well suited when applied for steel cylindrical models as it was originally developed for paper cylinders.

Utilizing the same FE model but with material properties of paper as described in earlier sections, DF buckling is simulated for four different cylinder radius i.e. 25, 35, 45 and 55 mm. Similar to the earlier case the critical stress is compared with the results from equations (1), (2) and (3). To isolate the effect of cylinder radius, the models are analyzed for the same geometry of diamond fold buckling (conforming buckling shape or the same number of diamond fold buckling

cell) and the buckling mode are as shown in Figure (15):

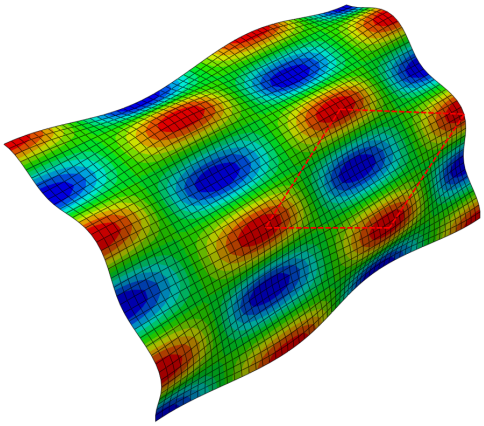

(a) Eigenmode of diamond fold buckling for a cylinder radius of 25 mm

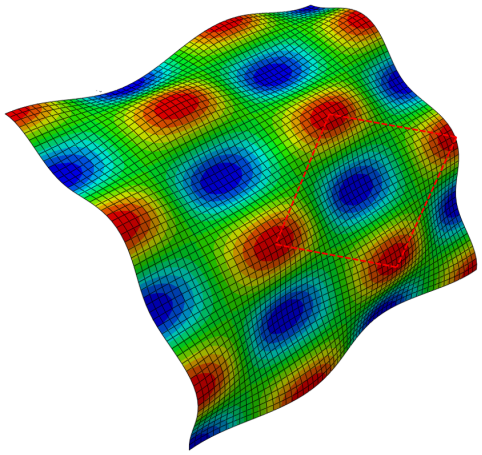

(b) Eigenmode of diamond fold buckling for a cylinder radius of 35 mm

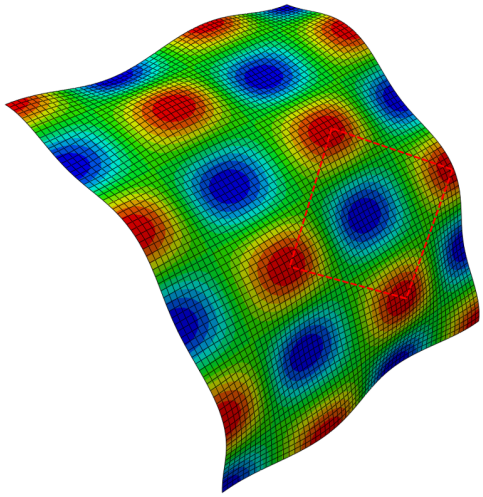

(c) Eigenmode of diamond fold buckling for a cylinder radius of 45 mm

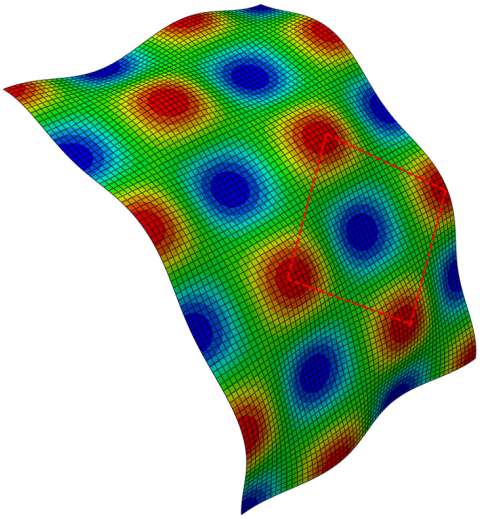

(d) Eigenmode of diamond fold buckling for a cylinder radius of 55 mm

Figure 15: Eigenmode of diamond fold buckling for different cylinder radius

In the Donnell model i.e. in equation (2) the value for E is taken to be the Young's modulus in the CD direction as the load is applied in the axial direction which is parallel to the CD direction and the yield strength is around 20 MPa. For obtaining the critical stress from the Pirelli equation i.e. Eqn (3), E_Θ and E_Z must be equated to the Young's modulus in the MD and CD direction respectively.

Figure (16a) shows the force vs displacement curve for all the four cylinder radius and it can be noticed that the displacement at buckling is different for all the four models but the critical load is almost the same. As the cross-sectional area varies the resulting critical stress decreases with an increase in the radius.

Figure (17) shows the comparison of FE results with the critical stress obtained from the Eqns (1), (2) and (3). The same trend as in the steel specimen case is noticed as the critical stress decreases with an increase in the cylinder radius. While the classical buckling theory over estimates the critical stress by around 50% when compared to FE results, the Pirelli model is

very accurate in its prediction and the FE results are in good agreement with the Pirelli model. Donnell model shows a difference of around 10-20% when compared with the FE results.

Analyzing both the cases of steel and paper material properties, it is evident that there is no one model which is applicable for both the cases. As expected, the classical buckling theory over estimates the critical stress for both the materials since it is more like an upper limit of buckling. Pirelli is suitable for anisotropic materials but limited with elastic buckling, whereas Donnell takes into account plastic yield (inelastic deformation) but assumes isotropic material behaviour. Therefore, in the case of paper (with strong anisotropy but with limited plastic deformation), Pirelli model fits better than Donnell. In conclusion, the analysis gives a better understanding about the pros and cons of the theoretical and empirical models.

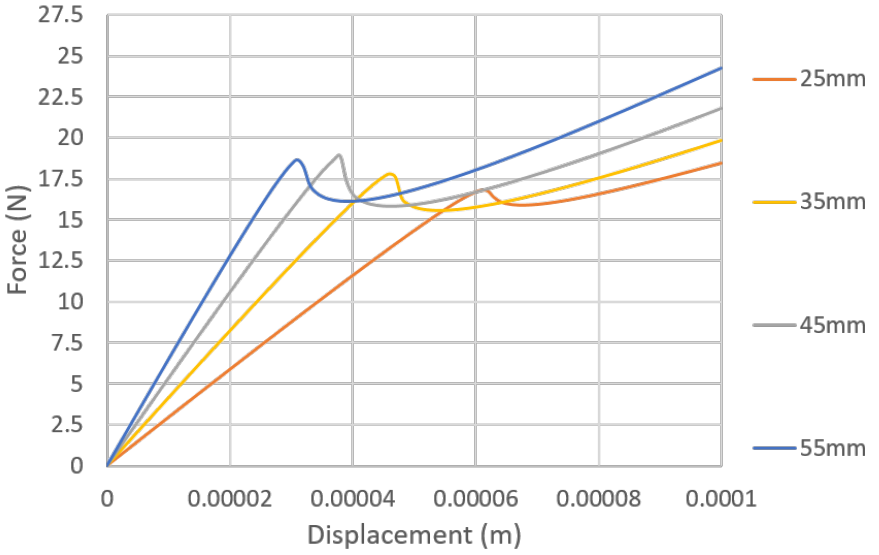

(a) Force vs displacement response for cylinder radius of 25, 35, 45 and 55 mm

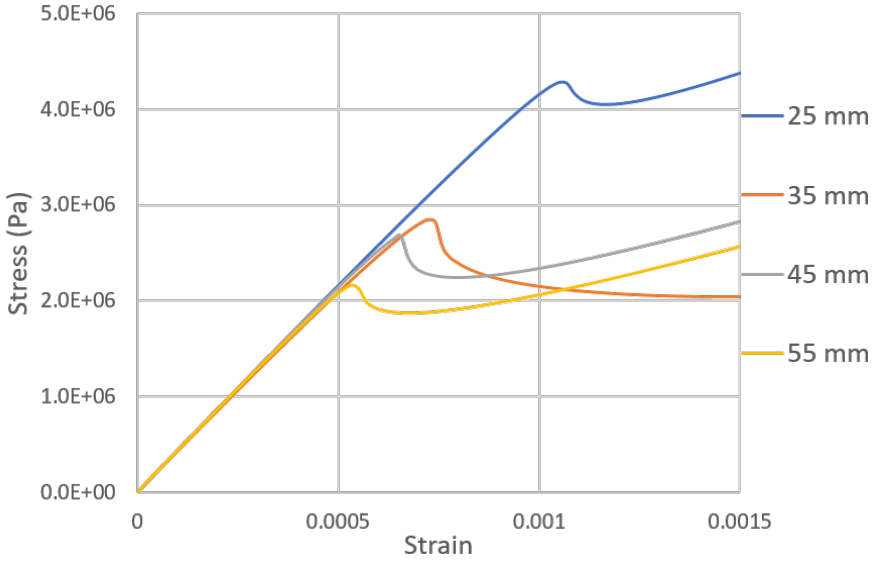

(b) Stress-strain response for cylinder radius of 25, 35, 45 and 55 mm.

Figure 16: FE results for the variation of critical stress due to cylinder radius

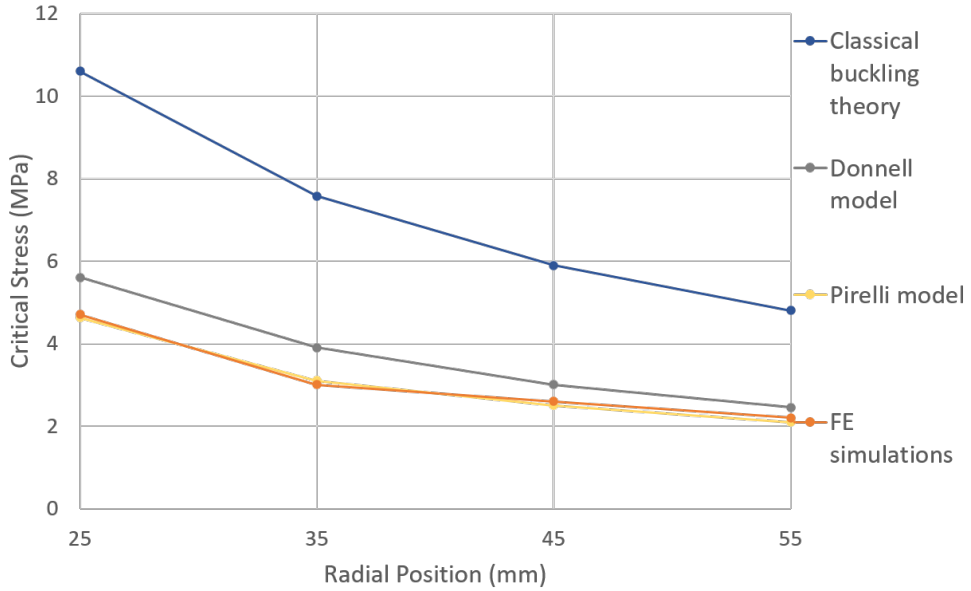

Figure 17: Variation of critical stress with cylinder radius for paper material properties. Comparison of critical stress from equations (1), (2), (3) and FE simulations

5.3 The effect of paper or cylinder thickness

Looking back on equations (2) and (3), it is clear that the critical stress is proportional to the thickness of the cylinder and inversely proportional to the radius of the cylinder. In order to investigate the effect thickness of the cylinder has on the critical stress, FE simulations were carried out for four different thickness of the cylinder i.e. 0.05, 0.1, 0.15 and 0.2 mm. The critical stress obtained from FEM was compared with the Donnell and the Pirelli models and is as shown in Figure (18).

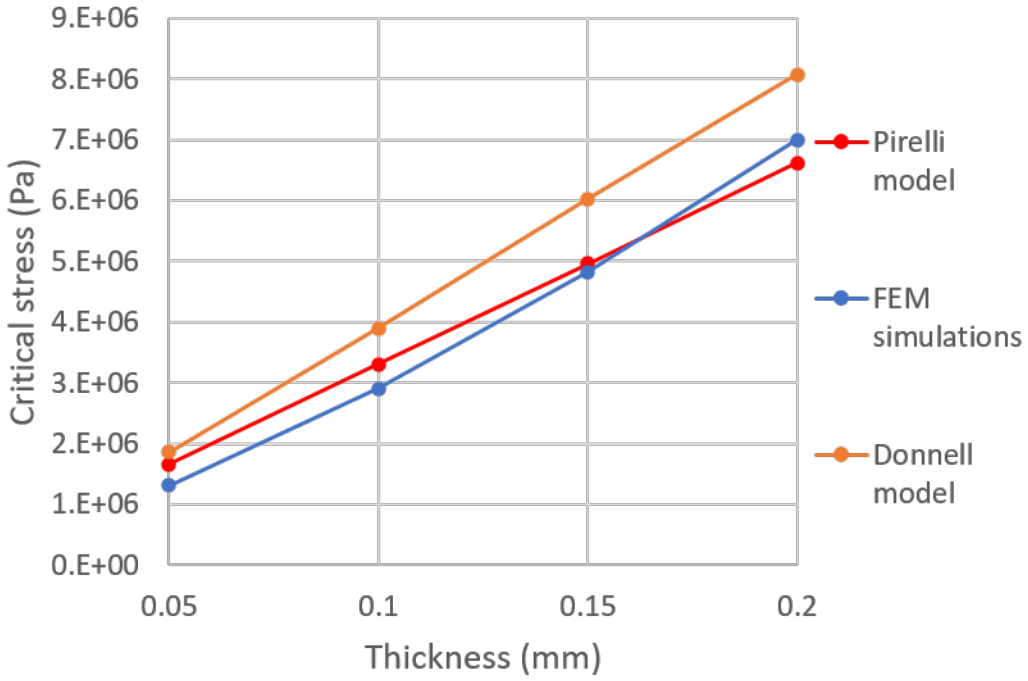

Figure 18: Variation of critical stress w.r.t thickness of thin cylinder

As the thickness of the shell or the cylinder increases the buckling strength of the cylinder increases i.e. thicker the cylinder greater is the resistance offered by the cylinder to the compressive load. The curve for the critical stress by Donnell and Pirelli, show a linear behaviour i.e. as the thickness of the paper increases there is a linear increase in the critical stress for buckling. Even-though the critical stress from FE simulations do not exhibit a linear response, it does verify the fact that the critical stress increases with the thickness of the cylinder or shell.

To conclude, the analysis verifies that thickness of the cylinder affects the buckling behaviour of the cylinder. Buckling strength of the thin-walled cylinder increases with increasing thickness of the shell.

6 Diamond fold buckling of multi-layer cylinder

In this section, the onset of diamond folds (the critical stress) will be analyzed for various number of layers. In addition to the number of layers, a parametric study will be conducted for quantifying the effects of contact properties, i.e. radial interfacial pressure and friction coefficient, onto the overall critical stress. The analysis for multi-layer cases is conducted with the same diamond fold configuration as in the previous section, as shown in Figure (12b). The analysis is carried out for four FE models consisting of up to four layers of continuous thin cylinder geometry. The layers are stacked with contact taken into account.

Surface interaction with a friction coefficient of 0.5 is defined between the layers. The layers are allowed to separate after coming into contact. Figure (19a) shows the force vs strain curve for one, two, three and four layers and the resulting stress vs strain curve is as shown in Figure (19b).

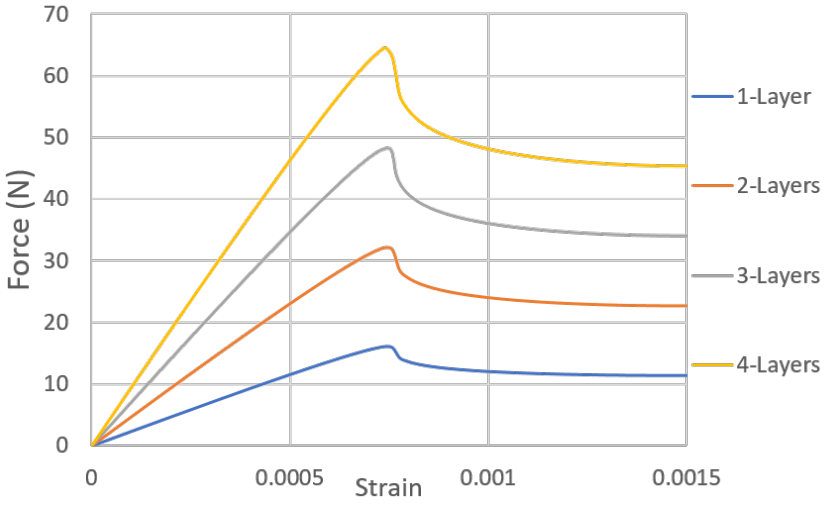

(a) Plot of force vs strain for one, two, three and four layers continuous cylinder model

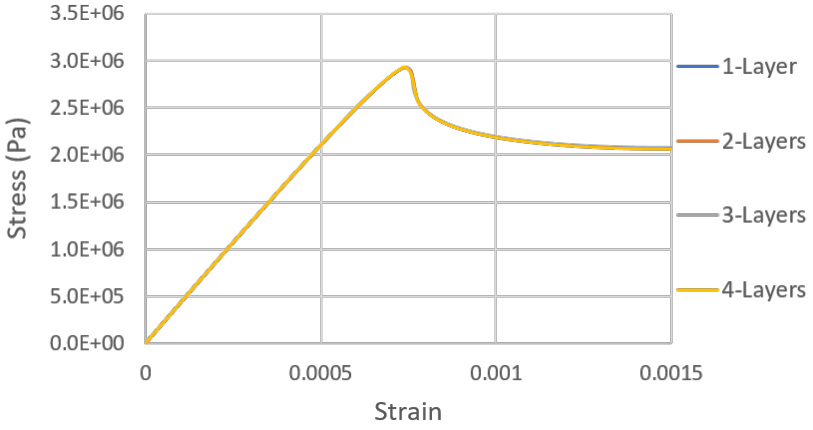

(b) Stress strain response of one, two, three and four layers continuous cylinder model

Figure 19: Plots of simulation results for the one, two, three and four layers continuous cylinder model

It can be seen from Figure (19a) that the force-displacement responses for multi-layer cylinder are proportional with the number of layers. This is indicated by the fact that the axial stress-strain responses for multi-layer cylinder are virtually identical to the single layer response.

In this analysis the layers are just stacked up on each other with contact definitions but no external pressure is applied to build contact pressure between the layers. Figure (20) shows the radial contact pressure is zero for a case of FE model with four layers before the application of compressive force. Therefore, in the absence of radial interfacial pressure, the overall diamond fold buckling behaviour of multi-layer cylinder is the same as the single layer response. The effect of interfacial pressure on the critical stress is investigated in the section to follow.

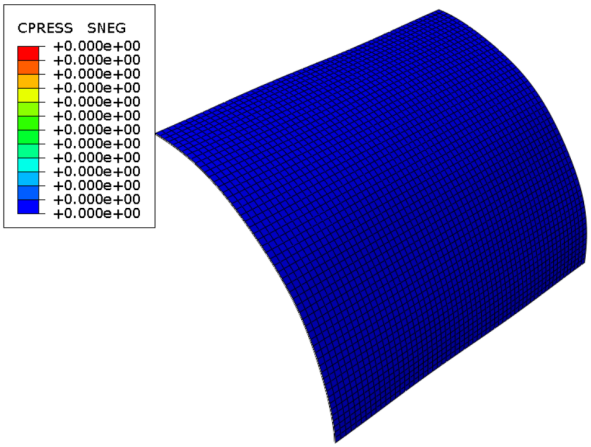

Figure 20: Contour of contact pressure before application of compressive load in a FE model with multi-layers

6.1 The effect of radial interfacial pressure

The effects of radial interfacial pressure on the overall diamond fold buckling response are studied by performing a sensitivity analysis on multi-layer cylinder with varying interfacial pressure (up to 1 MPa). This applied external pressure resembles the contact pressure created as a result of lapping tension. External radial pressure is applied equally on both interior and exterior sides of the cylinder. Figure (21b) shows the application of external pressure on the multi-layer cylindrical model.

Figure (22) depicts the stress-strain response for varying interfacial pressure for all the four models. The critical stress in the case of a single layer remains constant even with an increase in the radial interfacial pressure. This trend of constant critical stress is noticed because there is only one layer of paper and the model doesn't have any contact pressure or contact interactions. Since the external pressures are applied in opposite directions to each other, they nullify each others effect.

In contrast to the single layer, critical stress in the case of two, three and four layers increase with increase in the radial interfacial pressure and the results are as shown in Figure (23). Increase in radial interfacial pressure leads to increase in the shear resistance between the layers. Since shear resistance directly influences the buckling strength of the model, increased compressive force is required to buckle the model. In conclusion, both number of layers and interfacial pressure are factors which influence the critical stress of an axially compressed cylinder is verified from this part of the analysis. Findings from this study will be carried forward and extended to diamond folds buckling in stacked paper strip model which resembles an actual MI cable insulation.

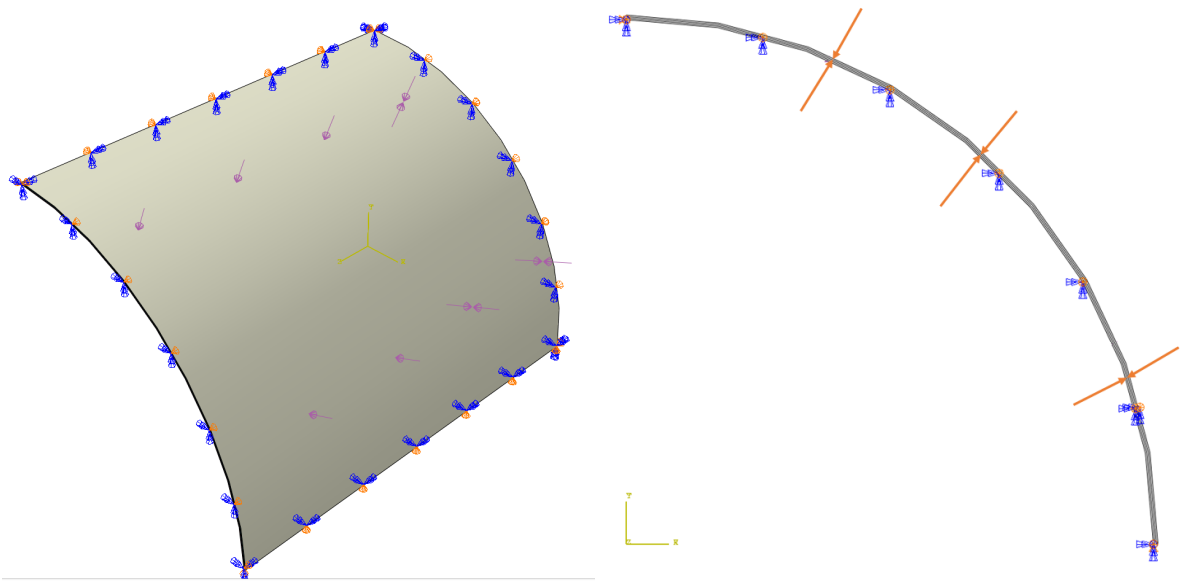

(a) Iso view of FE model

(b) Representation of the application of external radial pressure on the layers

Figure 21: FE model consisting of four layers of continuous cylinder geometry stacked up on each other. Arrows indicate the application of external pressure

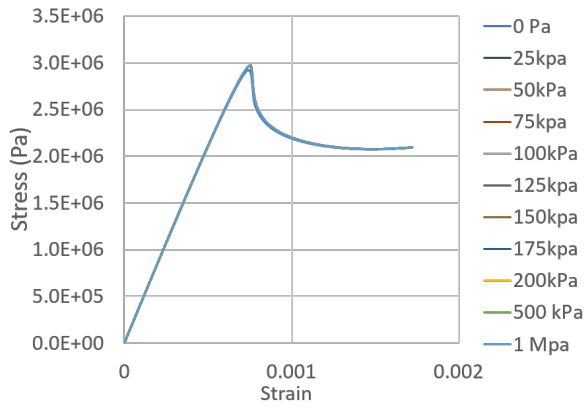

(a) One layer

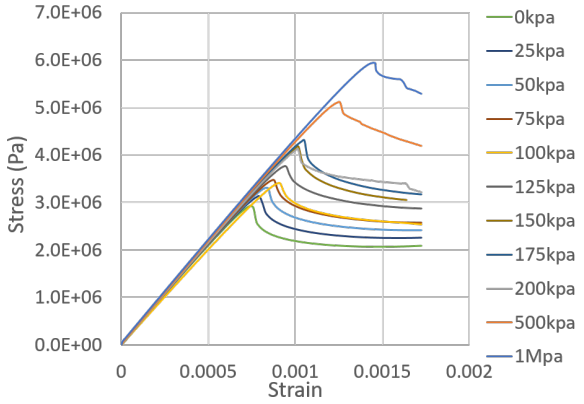

(b) Two layers

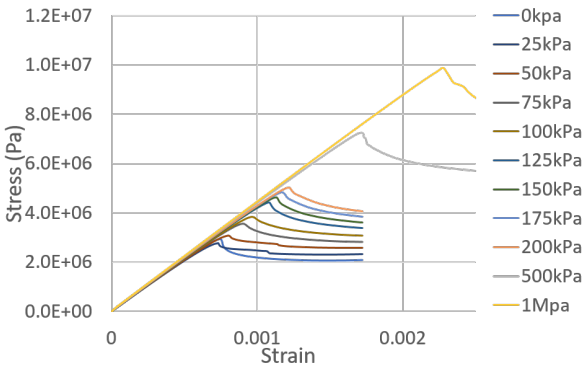

(c) Three layers

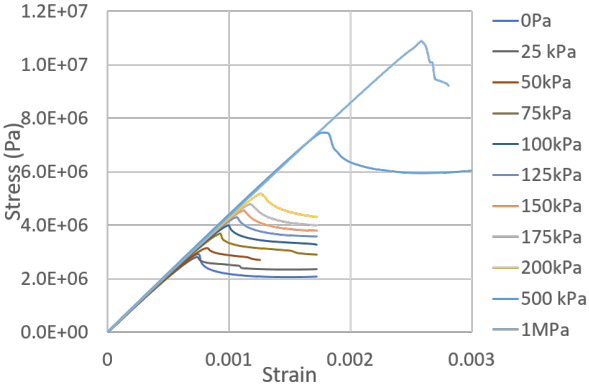

(d) Four layers

Figure 22: Stress-strain response for variation of interfacial pressure for one, two, three and four continuous cylinder layers

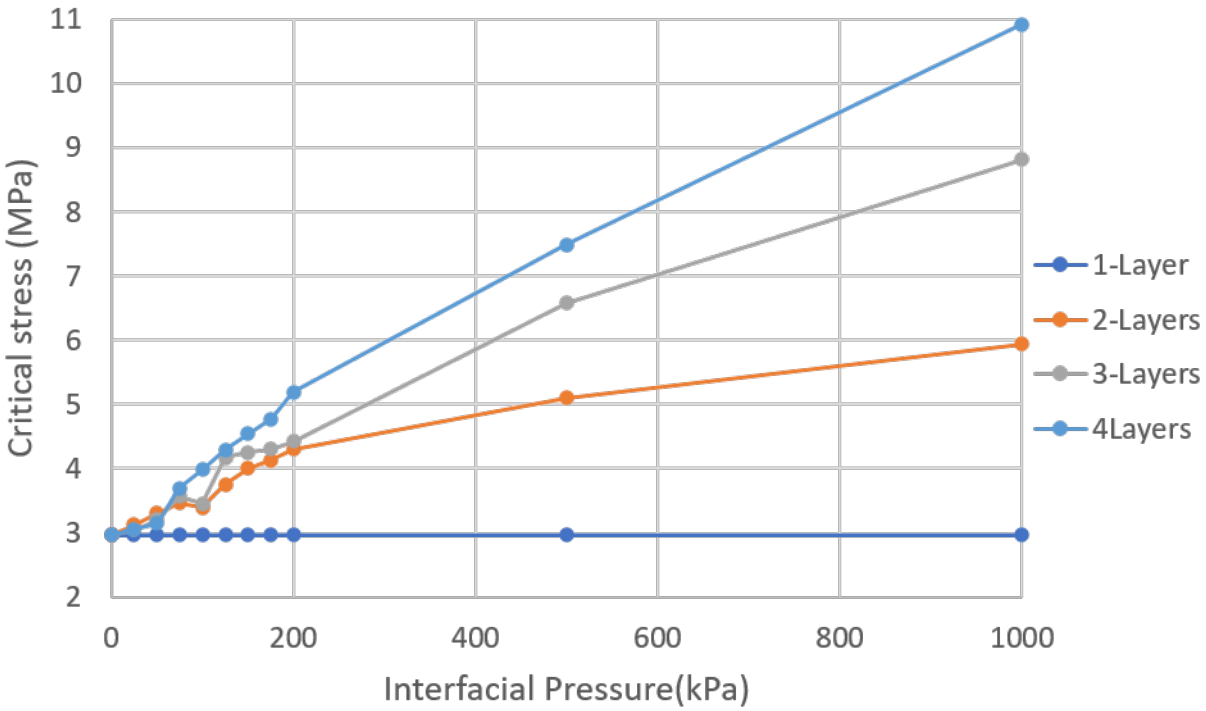

Figure 23: Effect of interfacial pressure on the critical stress for the case of one, two. three and four continuous cylinder layers

6.2 The effect of the paper friction coefficient

In order to investigate the effect of friction coefficient between paper layers, a FE model consisting of four layers of continuous thin cylinders is considered and the radius of the innermost layer is 35 mm. Surface interactions are formulated between the layers. Friction coefficient is varied from 0 to 2 with a step size of 0.25. External radial pressure is applied on the layers such that the radial interfacial pressure between the layers is constant at 100 kPa.

The stress strain response for variation of friction coefficient is as shown in Figure (24a). The critical stress is obtained from each of the responses and is plotted against the friction coefficient, the resulting trend is as shown in Figure (24b). The trend as seen in Figure (24b) clearly showcases an influence of friction coefficient on the critical stress. As the friction coefficient increases, there is a linear increase in the critical stress of the model.

When the friction coefficient is zero, the frictional forces between the layers is also zero. The critical stress when the friction coefficient is zero remains the same as in the case of a single paper layer i.e. 2.9 MPa. This shows that the number of layers and radial interfacial pressure has no effect on the critical stress if there doesn't exist any frictional forces between the layers.

The subsequent increase in critical stress w.r.t friction coefficient can be attributed to increase in shear resistance between the layers. For a model with a higher coefficient of friction, the critical stress will be higher due to the increased shear resistance between the layers, when compared to a model with lower friction coefficient. Hence, increase in friction coefficient leads to increase in the buckling strength of the model.

To conclude, the results from the analysis gives an insight as to how the coefficient of friction affects the diamond fold buckling behavior in a multi-layer continuous cylindrical model.

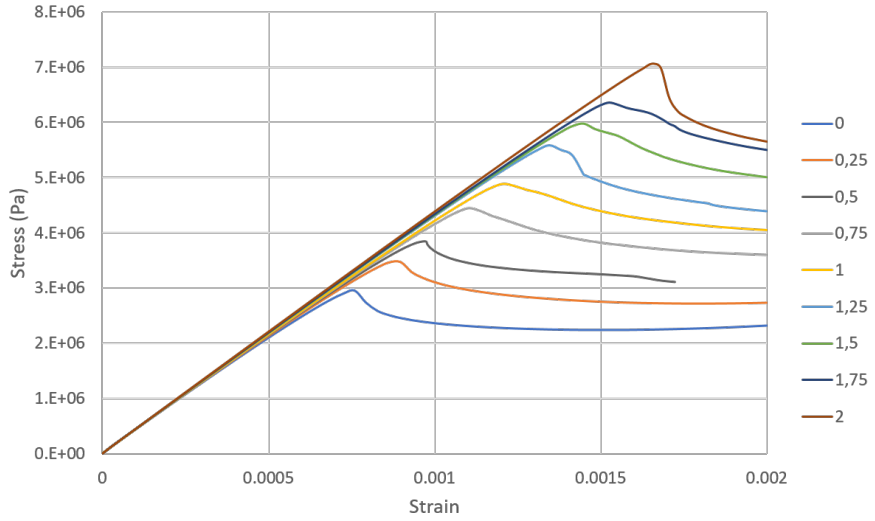

(a) Stress strain response for variation of friction coefficient

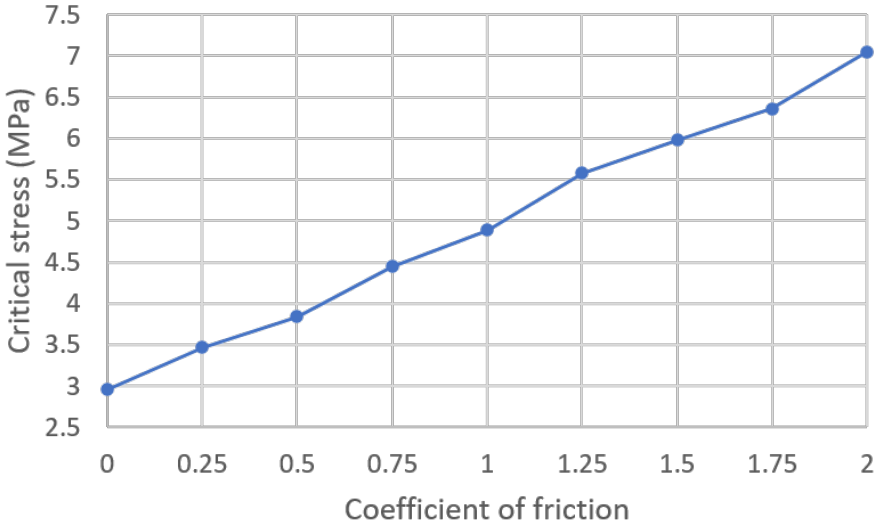

(b) Plot of critical stress vs friction coefficient

Figure 24: FE simulation results depicting the influence of the friction coefficient on the critical stress of the model

7 Diamond fold buckling of stack of paper strips with butt-gaps

The hypothesis for this thesis was defined assuming that the factors such as number of layers, coefficient of friction and interfacial pressure have an influence on the critical stress of a thin walled paper cylinder and the analysis uptill now have verified these assumptions for a case of a simplified version of the paper insulation in an MI cable. Since the main focus of thesis is to understand the cumulative effect of these factors on diamond fold buckling in an dry lapped paper insulation of an MI cable, a FE model with four layers of stacked paper strips with butt-gaps are simulated. The radius of the innermost layer is 35 mm.

The main difference between the FE model for this analysis and the FE model for four layers analyzed in the previous section, is the introduction of butt-gap of 2 mm between consecutive paper strips in the axial direction and also introducing registration of approximately 30%-70% between the layers. The effect of registration on the diamond fold buckling behaviour will be investigated in the section to follow. The FE model used for the analysis is as shown in Figure (25).

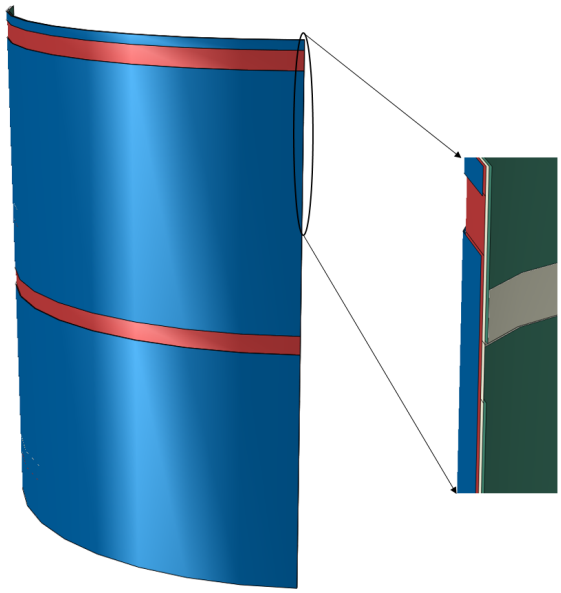

Figure 25: Four layers of stacked paper strips with butt-gaps and registration

Surface interactions are formulated between the layers. From the previous analysis it is established that the friction coefficient affects the critical stress of the model, hence for this case a constant value of 0.5 is defined. External pressure is applied to the layers, in the same way as in the investigation of interfacial pressure case. Application of external pressure on the paper layers, builds contact pressure between the layers. The effect of interfacial pressure is studied only in the range between 50 kPa and 200 kPa, as this range corresponds to the range of interest. Figure (26) shows the stress vs strain response for variation of interfacial pressure.

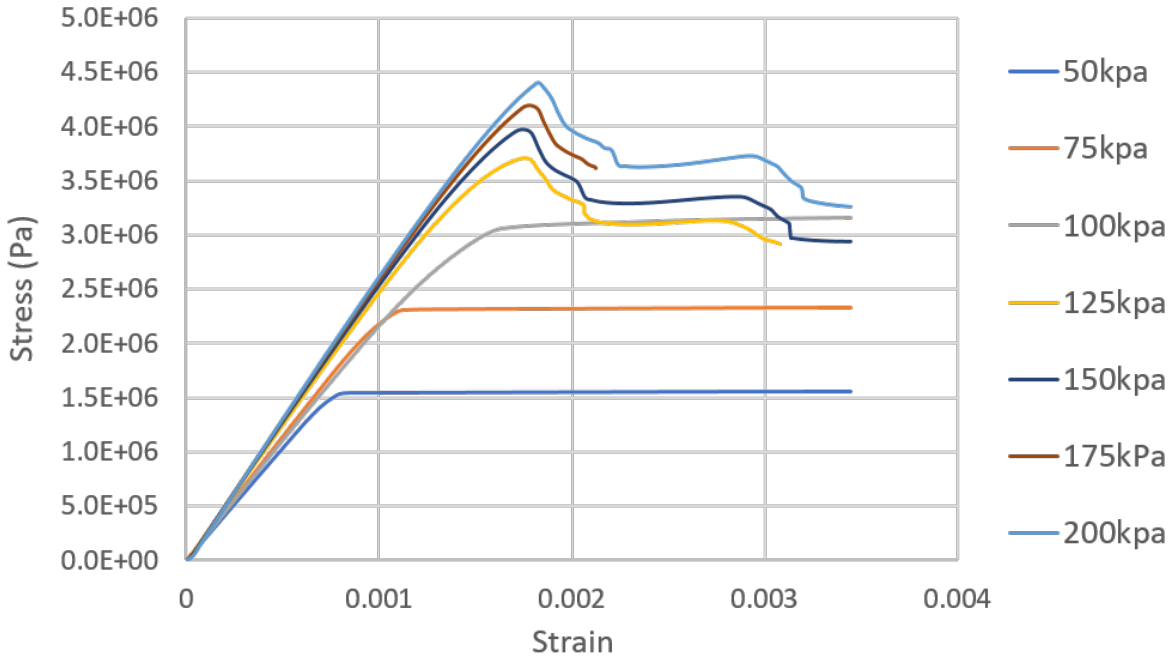

Figure 26: Stress strain response of the stack of paper strips with butt-gaps model for variation in interfacial pressure

In the case of a continuous cylinder model with multi-layers, when the compressive force in the axial direction reached its critical point, the cylinder would buckle into diamond folds irrespective of the interfacial pressure between the layers. However, in the case of stack of paper strip with butt-gaps, if the onset of slip is lower than the critical buckling load, paper strips will slip first and result in a slipping behaviour as shown in Figure (27a). The onset of slip initiation depends on contact pressure between the layers, area of contact and the coefficient of friction. Slipping takes place over the smaller area corresponding to the shorter side of the registration i.e. over the area corresponding to 30% in this case. Slipping behaviour is observed for lower radial interfacial pressure (below 100 kPa). Since axial stress is relatively constant during slipping, paper strips will continuously slip until butt-gaps are fully closed before diamond fold buckling can take place. In general, the condition for slipping to occur is that, axial force must be greater than the force for slip initiation but must be lower than the critical force at which buckling might occur.

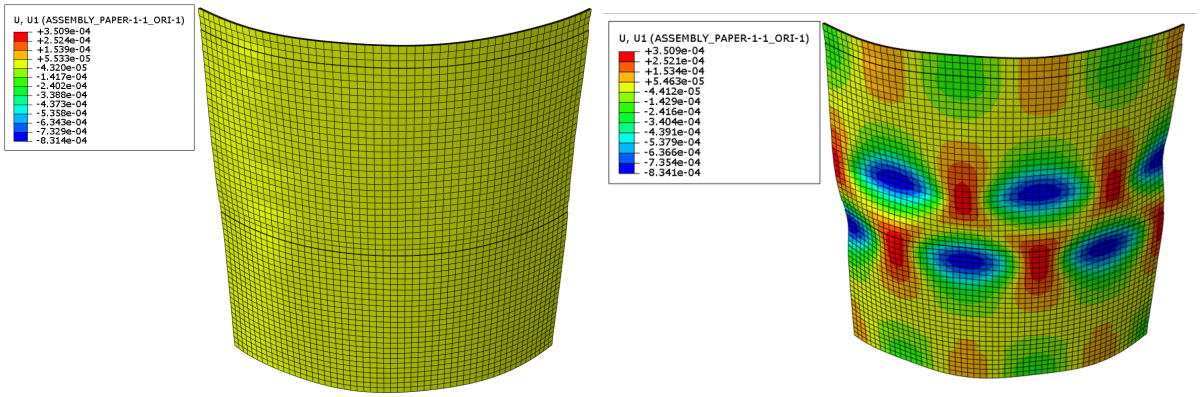

(a) Slipping behaviour

(b) Buckling behaviour

Figure 27: Example of the slipping and buckling behaviour observed in the stacked paper strips with butt-gaps model. Color contour indicates radial displacement

At radial position of 35 mm, the transition from slip-dominated behaviour to diamond fold buckling dominated response is obtained at radial interfacial pressure between 100-125 kPa. This is because when the interfacial pressure increases the force at slip initiation also increases but the critical force for bucking is still lower than the force at slip initiation. Hence, the model buckles instead of slipping. So the condition for diamond fold buckling is that the compressive force must be greater than the critical force for buckling but lower than the force at slip initiation.

Contact pressure between layers is a result of lapping tension in the MI cable insulation and the results suggest that lapping tension plays an important role in deciding whether the paper insulation will undergo the variable butt-gap or diamond fold buckling phenomenon. For a lapping tension below 100 kPa the insulation will undergo variable butt-gap phenomenon and after a certain lapping tension (between 100-125 kPa) it will undergo diamond fold buckling. Hence in order to prevent the paper insulation system from undergoing diamond fold buckling, the lapping tension has to be carefully controlled such that it is lower than the critical range.

7.1 The effect of butt-gaps

The effect of interfacial pressure on critical stress for the continuous cylinder configuration with four layers has been studied in the section *effect of radial interfacial pressure*. The critical stress from this case is comparable with the critical stress obtained for the stack of paper strips with butt-gaps, as they differ only in terms of butt-gaps. Figure (28) shows the comparison between the continuous and stacked paper strips with butt-gaps configurations. The grey line in Figure (28) indicates the critical stress for diamond fold buckling in the stack of paper strips with butt-gaps model.

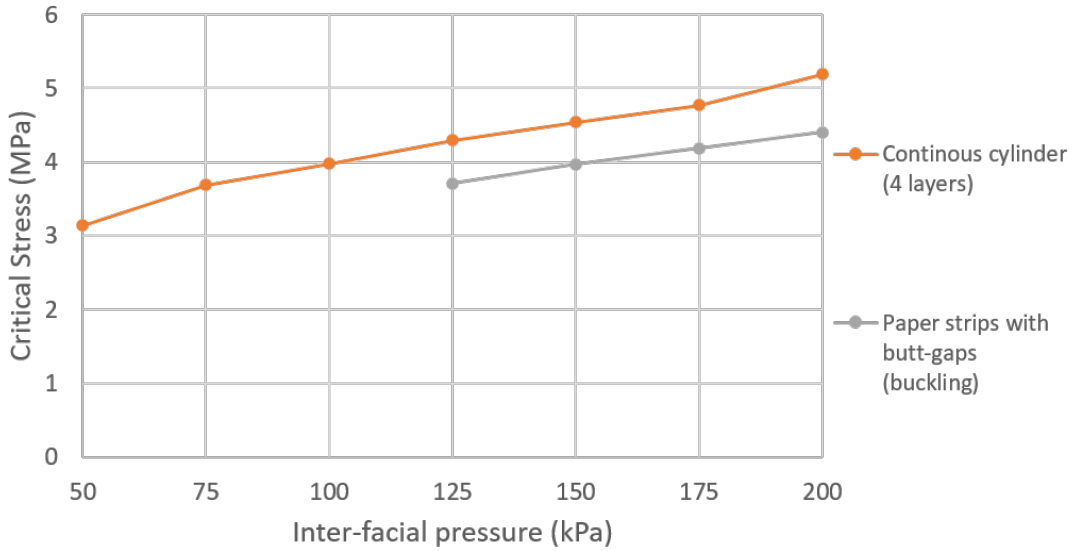

Figure 28: Comparison of critical stress results for variation of interfacial pressure for continuous cylinder (four layers) and stacked paper strips with butt-gaps configurations

From Figure (28), it is seen that there is approximately 10-15% drop in the critical stress of the model due to the introduction of butt-gaps and registration. It is clear from this comparison that the butt-gap model is less stiff than its counterpart i.e. continuous cylinder model. The main reason for the reduction in stiffness can be attributed to the loss of material by the introduction of butt-gaps. Butt-gaps are regions of stress concentration and generally the model buckles around the region of the butt-gaps. Due to the loss of material, the region around them are more vulnerable to the compressive load than other regions.

Continuous cylinder model behaviour is the upper bound for paper strip response under axial compression i.e. the continuous cylinder is equivalent to stack of paper strips without butt-gaps.

7.2 The effect of registration or overlaps area

In the section *Diamond fold buckling of stack of paper strips with butt-gaps* above, the analysis was carried out for a registration scheme of 30-70% as shown in Figure (29a) and the variation of critical stress due to interfacial pressure was studied. In this section, in order to understand the effect of registration on the critical stress, a new registration scheme of 25-75% as seen in Figure (29b) was used. The length of the shorter side i.e. W_{P1} is reduced from 30% to 25%. Interfacial pressure was varied to understand its effect on the critical stress of the model and the resulting critical stress comparison for both the cases is as shown in Figure (30). Critical stress behaviour for the continuous cylinder with four layers is also compared with the results from the registration models.

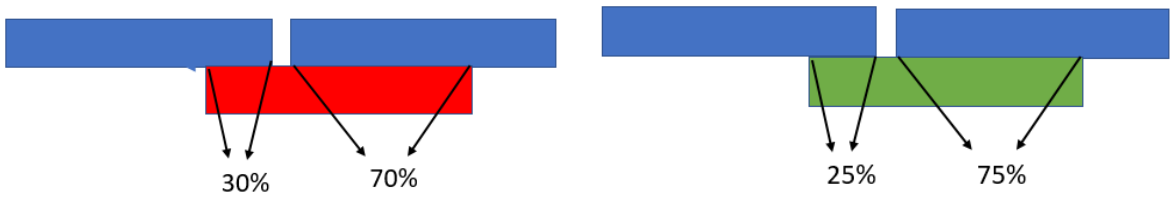

(a) Registration scheme of 30-70%. Ratio of W_{P1} to W_{P2} is 30/70

(b) Registration scheme of 25-75%. Ratio of W_{P1} to W_{P2} is 25/75

Figure 29: Schematic representation of the registration schemes utilized in the analysis

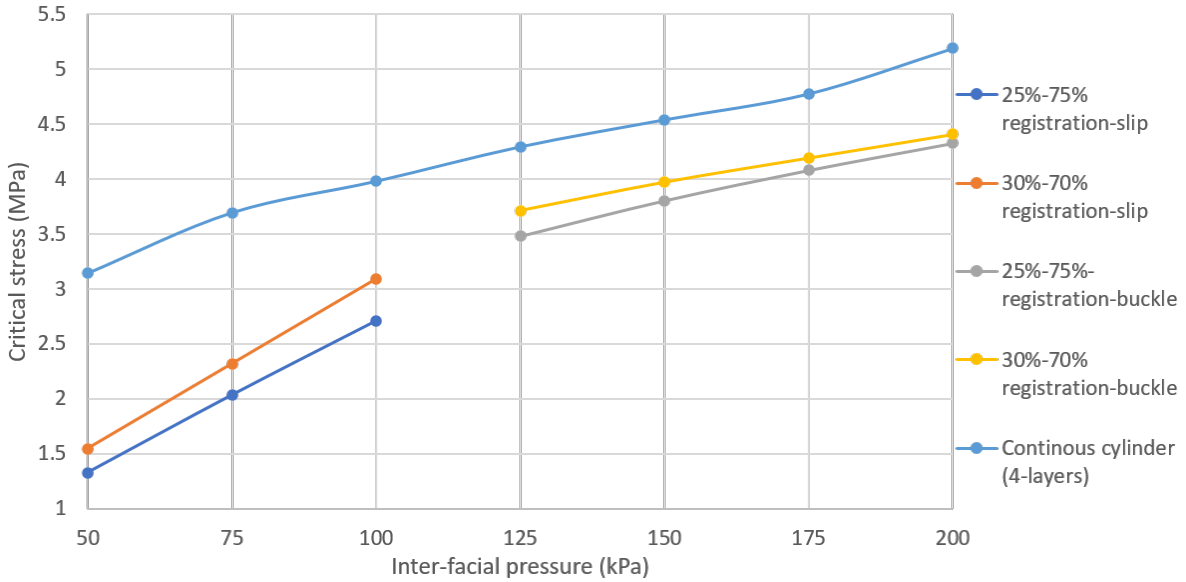

Figure 30: Comparison of critical stress results from continuous cylinder (four layers), 30-70% and 25-75% registration model, for variation of interfacial pressure

The blue and orange curves respectively in Figure (30) indicate the critical stress for slipping behaviour in the 25-75% registration model and 30-70% registration model respectively, while the yellow and grey curves represent the critical stress for buckling in the 25-75% and 30-70% registration models respectively.

As in the earlier case the continuous cylinder behaviour acts as an upper limit for the paper strip response under axial compression. Both in the slipping and in the buckling behaviour, critical stress is lower for the 25-75% registration scheme than the 30-70% scheme. Irrespective of the behaviour, as the width of the shorter side (W_{P1}) decreases, the area corresponding to the side W_{P1} also decreases. Reduction in area corresponds to decrease in the force required to overcome the slipping resistance and hence a drop in the critical stress is seen. Conversely, if the width of the shorter side (W_{P1}) increases, the critical stress increases because the area corresponding to the shorter side also increases, which in turn increases the slip resistance and hence would the force required to buckle or initiate slip in the model increase.

In conclusion, this section gives an understanding as to how the critical stress of the paper insulation is also dependent on the registration scheme applied between the paper strips.

8 Conclusions

Numerical FE modelling and simulation has been used to study the effects of material properties, paper thickness, radial interfacial pressure, registrations, etc, on the overall response of MI cable insulation during diamond fold buckling.

For a continuous cylinder geometry critical stress of buckling is not directly affected by the number of layers but in combination with interfacial pressure, they affect the diamond fold buckling behaviour in the cylindrical models. Thus for a constant interfacial pressure, critical stress of the model increases non-linearly with increase in the number of layers.

The coefficient of friction between the layers in paper insulation, plays a significant role in the diamond fold buckling behaviour. The higher the coefficient of friction, the higher is the shear resistance between the layers, which leads to an increase in the critical stress of buckling. Similarly, interfacial pressure also has a direct influence on the critical stress of the cylinder.

For a stack of paper strips with butt-gaps model which closely resembles the insulation of an MI cable, if the number of layers, registration and the coefficient of friction is kept constant, it is the lapping tension which determines the behaviour of the model. If the lapping tension is below a critical value, the paper strips in the model will slip over each other, leading to variable butt-gaps and if it exceeds the critical value the model will undergo diamond fold buckling phenomenon.

Hence, in an MI cable insulation the parameters lapping tension, coefficient of friction, number of layers, registration and butt-gaps have to be carefully controlled so as to minimize the risk of diamond fold buckling phenomenon occuring.

References

[1] NKT, "Cable solutions-high, medium, low voltage cables; accessories", Retrieved May 13, 2021, from https://www.NKT.com/

[2] Ljumba N, *High voltage cable insulation systems*, EE publishers, May. 2008

[3] M. J. P. Jeroense and F. H. Kreuger, *Electrical conduction in HVDC mass-impregnated paper cable*, IEEE Transactions on Dielectrics and Electrical Insulation, vol. 2, no. 5, pp. 718-723, Oct. 1995, doi: 10.1109/94.469968.

[4] Kuffel, E., Zaengl, W.S., Kuffel, J. (2000). "High Voltage Engineering (2 ed.)", Butterworth Heinemann/Newnes, ISBN 0-7506-3634-3.

[5] Priaroggia, P. G., Occhini, E., amp; Palmieri, N, "Fundamentals of the theory of paper lapping of a single core high voltage cable," Milano: Pirelli, pp 104-125,1961,

[6] Fung Y, Sechler E, *Buckling of thin-walled circular cylinders under axial compression and internal pressure*, Journal of the aeronautical sciences, 24(5):351â356, 1957

[7] Koshnitsky, N. S. , "Classical solution to the buckling of a thin cylindrical shell," Master's thesis, University of Adelaide, pp. 1-20, November, 1982

[8] Timoshenko, S. P., amp; Gere, J. M. , "Theory of elastic stability," New York: McGraw-Hill Book, Buckling of shells, 1961

[9] Donnell, L. H.,"A new theory for the buckling of thin cylinders under axial compression and bending," Pasadena: Guggenheim Aeronautical Laboratory, 1934

[10] Batdorf S.B., Schildcrout .M., Stein .M., *Critical Stress of Thin-Walled Cylinders in Axial Compression*, National Advisory Committee for Aeronautics/NASA, August 1968

[11] Dassault systems, "Abaqus/Standard users manual, version 6.14, Introducing a geometric imperfection into a mode", 2019.

[12] Kröling, H., Endres, A., Nubbo, N., Fleckenstein, J., Miletzky, A. and Schabel, S., *Anisotropy of paper and paper based composites and the modelling thereof*, ECCM16, pp.1-8, 2014,

[13] Aggarwal K., Wu S, Papangelis J., "Finite element analysis of local shear buckling in corrugated web beams," Engineering structures,162 : 3750, 2018

[14] Dassault systems, "Abaqus/Standard users manual, version 6.14, Elements library," 2019.

[15] Dassault systems, "Abaqus/Standard users manual, version 6.14, Unstable collapse and postbuckling analysis," 2019.